공학석사 학위논문

Synthesis, Characterization, and Applications of Highly Efficient Far-Red to Near Infra-Red Emissive β-Dicyanodistyrylbenzene Derivatives

고효율의 근적외선 영역의 발광특성을 보이는 베타 다이사이아노다이스티릴벤젠 유도체들의 합성, 특성분석, 그리고 응용에 관한 연구

2014년 2월

서울대학교 대학원

재료공학부

김 민 아

Synthesis, Characterization, and Applications of Highly Efficient Far-Red to Near Infra-Red Emissive β-Dicyanodistyrylbenzene Derivatives

고효율의 근적외선 영역의 발광특성을 보이는
베타 다이사이아노다이스티릴벤젠 유도체들의
합성, 특성분석, 그리고 응용에 관한 연구

지도 교수 박 수 영

이 논문을 공학석사 학위논문으로 제출함
2014 년 2 월

서울대학교 대학원
재료공학부
김 민 아

김민아의 석사 학위논문을 인준함
2014 년 2 월

위 원 장 _____ (인)

부위원장 _____ (인)

위 원 _____ (인)

Synthesis, Characterization, and Applications of Highly Efficient Far-Red to Near Infra-Red Emissive β-Dicyanodistyrylbenzene Derivatives

A THESIS SUBMITTED IN PARTIAL FULFILLMENT OF

THE REQUESTMENTS FOR THE DEGREE OF MASTER

IN ENGINEERING AT THE GRADUATE SCHOOL OF

SEOUL NATIONAL UNIVERSITY

February 2014

BY

Mina Kim

Supervisor

Prof. Soo Young Park

Abstract

Synthesis, Characterization, and Applications of Highly Efficient Far-Red to Near Infra-Red Emissive β-Dicyanodistyrylbenzene Derivatives

Mina Kim
Department of Materials Science and Engineering
The Graduate School
Seoul National University

In the last decades, the immense interest in highly fluorescent π-conjugated compounds which emit deep red to near infrared (NIR) in the solid state has been driven by their utilities toward advanced photonic applications such as organic light-emitting diodes, fluorescent chemosensors, organic solid-state lasers. However, most of organic red emitting fluorophores suffer from aggregation-caused quenching due to their characteristics of strong π–π stacking, dipole-dipole interaction or donor (D)-acceptor (A) charge transfer interaction. Thus, the

development of strongly far-red to NIR emitting materials in the solid state is still challenging.

Recently, highly fluorescent solid-state emitters based on 2Z,2'Z-3,3'(or2,2')-(2,5-dimethoxy-1,4-phenylene)bis(2(or3)- phenylacrylonitrile (MODCS) have been explored and contributed to establish the relationship between the molecular arrangement and the corresponding fluorescence features on aggregation-induced enhanced emission (AIEE) depending on the position of the pendant cyano group on the stilbene.

As an extended work for further development of β-MODCS exhibiting strong deep red-NIR fluorescence, I herein report the synthesis of the D-A-D-A-D type β-dicyanodistyrylbenzene (β-DCS) derivatives that have various N-amine moieties (β-MODEADCS, β-MODBADCS, β-MODPADCS, β-EODEADCS) with emission maximum peaks in the range of 650 nm and 718 nm. Among them, β-MODEADCS especially exhibits emission in the Near Infra-Red region with quite good quantum efficiency (Φ_{FL} = 0.42). These unique highly emissive properties in the solid-state were thoroughly investigated by UV-Vis spectroscopy, photoluminescence spectroscopy, fluorescence lifetime measurement, electrochemical measurement, and single crystal

X-ray analysis. Furthermore, we also present β-dicyanodistyrylbenzene based highly red fluorescent amphiphilic molecules β-EODEADCS and β-wedge DEADCS. Their optical properties and intriguing nanostructures in water were obtained by DLS, SEM, cryo-TEM experiments and UV-Vis spectroscopy. Based on the understanding of their optoelectrical characteristics, we demonstrated p-type single crystal organic field-effect transistors (SC-OFETs) using high crystalline β-MODEADCS and bio-imaging with self-assembled nanoparticles of β-EODEADCS.

Keywords: β-dicyanodistyrylbenzene, high fluorescence, red fluorophore, piezochromism, solid state, biological imaging

Student Number: 2012-22535

Contents

List of Tables

List of Schemes

List of Figures

Chapter 1. Introduction

1.1 Highly Efficient Solid-state Emissive π−conjugated Organic Materials

To design and synthesize highly emissive π-conjugated organic materials in the solid state is a fundamental and important prerequisite for realizing various optoelectronic and photonic applications, such as organic light-emitting diodes (OLEDs),[1] organic solid-state lasers,[2] and fluorescent sensors.[3] Though a great number of molecules show highly emissive property in dilute solution, the examples of organic fluorophores exhibiting intense solid-state emission are still quite limited owing to severe concentration quenching often resulting from certain intermolecular interactions.[4] These intermolecular interactions leading to the non-radiative deactivation process[5] include excitonic coupling, excimer formation, and excitation energy migration to the impurity trap. There have been many efforts to avoid fluorescence quenching in the condensed state effectively. Different molecular design strategies have been proposed to achieve an intensified solid-state emission. Tang and coworkers have introduced bulky substituents into the original fluorophore based on silole[6] or tetraphenylene[7] to hinder strong π-π interaction and observed aggregation-induced emission (AIE) driven by the restriction of intramolecular rotation in the aggregates.[8] Also, Park and coworkers have developed a wide range of π-conjugated organic molecules exhibiting extremely large fluorescence enhancement in the solid state

attributed to spatial confinement and formation of specific supramolecular stacking architecture, known as aggregation-induced enhanced emission (AIEE).[9a] During the last decades, though most H-aggregates have commonly been known to be low emissive, several highly fluorescent H-aggregates are recently reported. In single crystalline of H-aggregate, high quantum efficiency resulting from the small trap concentration and long mean path to the surface has been demonstrated.[9b] If exciton diffusion slows down, weakly exciton coupled polycrystalline H-aggregates (nanoparticles, films) might also show highly emissive properties in solid state.[9b] In addition, other approaches which include cross-dipole stacking,[10] dendritic protection, lateral attachment of steric bulky diarylamino or dimesityl groups to the π-conjugated framework to enhance intramolecular charge transfer (CT) transition[11] have also been used in establishment of new molecular design principle.

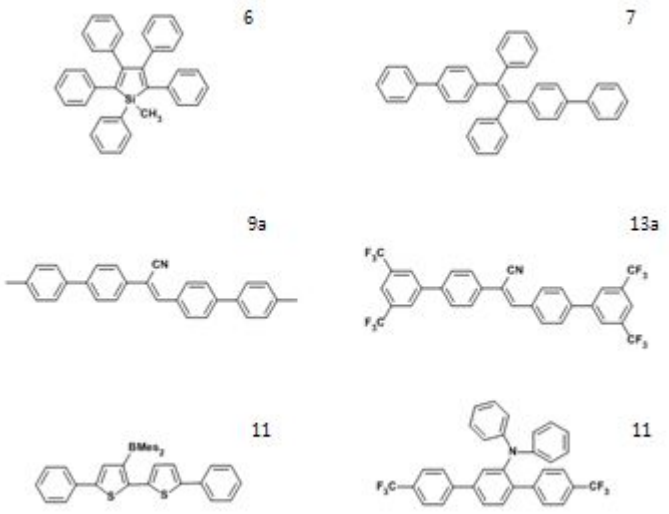

Scheme 1.1. Representative molecular structures exhibiting highly efficient solid-state emission.

1.2 Aggregation induced enhanced-emission (AIEE)

π-Conjugated organic materials are of great interest in various optoelectronic applications on account of their unique photophysical properties and diverse structural characteristics such as nano- and micrometer-sized self-assembly. Although many organic luminophores show high fluorescence in solution, the decrease of fluorescence efficiency in the solid state is quite general and is mainly attributed to strong π-π interaction which often leads to non-radiative decay pathway.[5] For the majority of π-conjugated molecules including stilbene, the molecular transition dipole moment μ is oriented along the long molecular axis.[12] Therefore, such molecules tend to form H-type aggregation where molecules are aligned parallel to each other with strong intermolecular interaction and induce concentration quenching (See Figure 1.1). Formation of H-type aggregate is characterized by blue-shifted absorption bands with respect to those of isolated molecule in solution because the higher transition state generated by electronic coupling is dipole-allowed state.[13] In contrast, some cyanostilbene derivatives show weak fluorescence in solution, whereas fluorescence intensity increases drastically in the solid state to give aggregation-induced enhanced emission (AIEE). [9] Such different fluorescence changes (concentration quenching vs AIEE) are correlated with the aggregation morphology. For instance, CN-MBE molecules (See Figure 1.2) have a twisted conformation by the steric effects in biphenyl unit and cyano group attached to vinylene moiety. Therefore, isolated CN-MBE molecules having twisted conformations in solution tend to suppress the radiative

process, thereby rendering the non-fluorescent property. The bulky and polar cyano group in CN-MBE, however, plays an important role in directing specific intermolecular interaction which results in J-type aggregation where the molecules are arranged in head-to-tail direction. In general, the J-aggregation absorption band is distinctively red-shifted because the lower optical transition is an allowed state (See Figure 1.1) which often appears as an intense narrow band.[14] Strong fluorescence of J-aggregate in both single- and polycrystalline samples is attributed to high radiative rates and slow exciton diffusion by weak J-type exciton coupling.[9b] Therefore, the cyanostilbene derivatives show aggregation-induced enhanced emission (AIEE) behavior due to the combined effects of aggregation-induced planarization and J-aggregate formation.

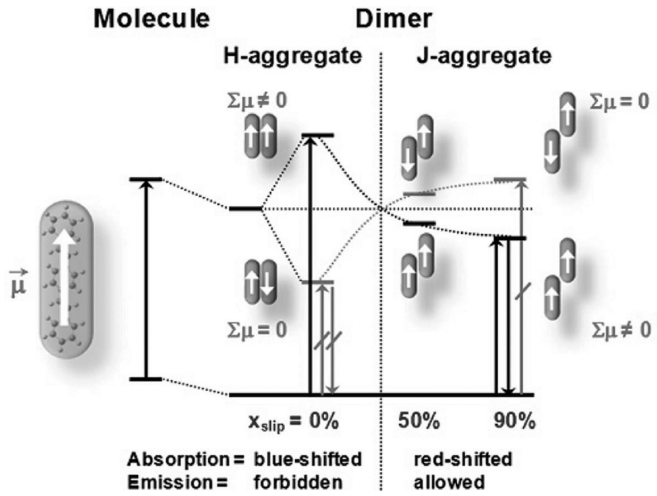

Figure 1.1. H- and J-aggregates and their influence on the absorption and emission processes in the framework of molecular exciton models. [9b]

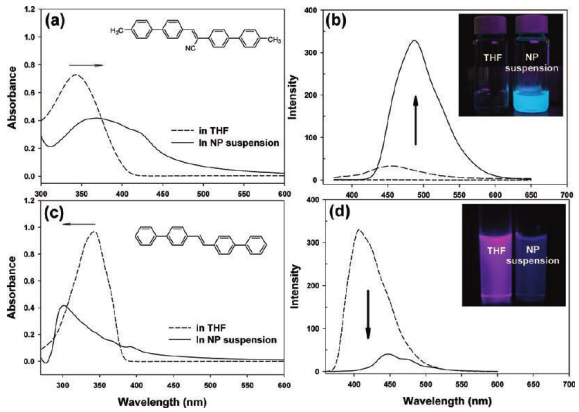

Figure 1.2. UV absorption and PL spectra of CN-MBE (a and b) and DPST (c and d) (2 x 10^{-5} M) in THF and NP suspensions in 80:20(v/v) water:THF mixture, respectively. [13a]

1.2.1 Organic field-effect transistors (OFETs)

Single-crystalline organic π-conjugated molecules have been studied intensively during the last decades.[15] Although electronic research fields utilizing inorganic materials are well established, development of organic semiconducting materials is still conducted continuously because of their remarkable benefits such as mechanical flexibility, light weight, and low cost. Especially, organic semiconductors using single crystals are suitable for OFETs due to simple solution process. Since the first report on the organic field-effect transistors (OFETs) in 1987,[16] the performances of device have been improved enormously. A field-effect transistor consists of three terminals in which the current through the organic semiconducting material flows between source and drain terminal. The current is controlled at the gate terminal by voltage that causes electric field through the dielectric. As shown Figure 1.3, there are two typical device configurations in OFETs; top contact and bottom contact.[17] So many p-type materials with high mobility have been developed based on the solution-processing. In contrast, the exploration of n-type material showing high performance is limited because of the difficulty in efficient electron injection, well ordered intermolecular stacking and high stability. Our group has explored dicyanodistyrylbenzene (DCS)-based materials with appropriate electric function and intense fluorescence. Among them, CN-TFPA including β position of cyano group was self-assembled into highly ordered 2-dimensional crystalline terrace structure, which was deposited on the substrate by solution-processing.[18a] The 2D crystalline layer

film OFETs showed a high electron mobility of up to 0.55 $cm^2 V^{-1}s^{-1}$ (See Figure 1.4 (a)). As shown Figure 1.4 (c), CN-TFPA exhibited two different crystalline polymorphs (G-phase, B-phase) with different slipped angle and each crystal has highly emissive property. Furthermore, ambipolar transport behavior was recently demonstrated by binary mixed CT crystals based on DSB (distyrylbenzene)/DCS (dicyanodistyrylbenzene) framework.[18b] Therefore, DCS derivatives were manifested as desirable design principle for OFETs.

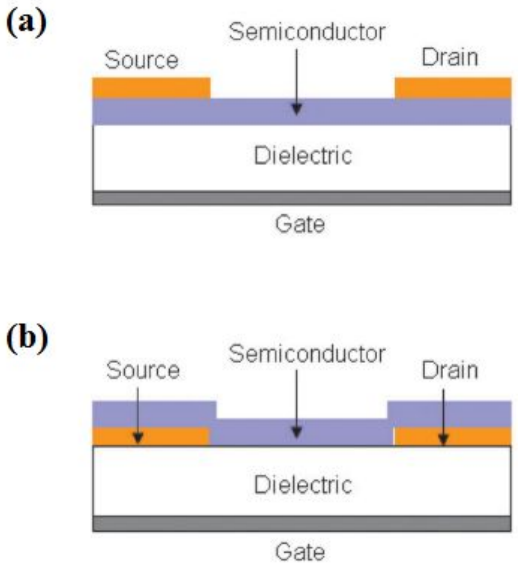

Figure 1.3. Schematic configuration of organic field-effect transistors (OFETs); (a) top contact, (b) bottom contact.

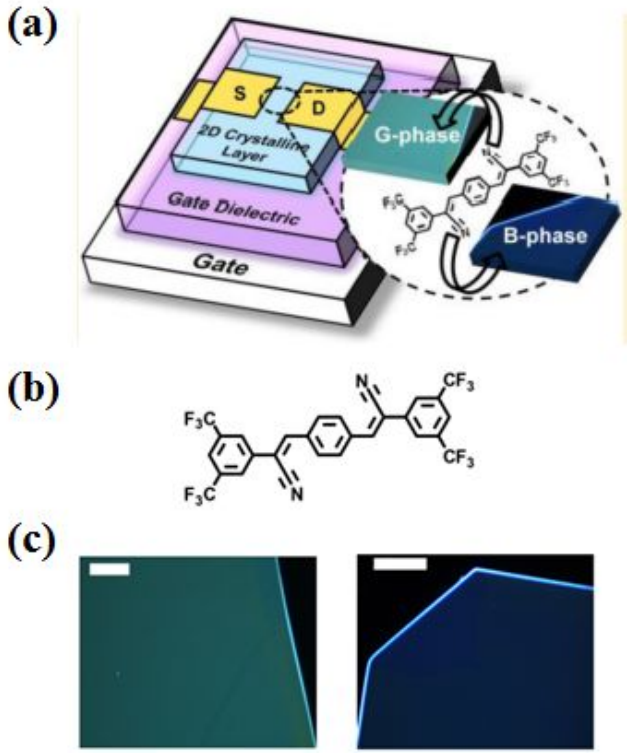

Figure 1.4. (a) Graphic illustration n-type single crystal OFET, (b) Molecular structure of CN-TFPA, (c) two phases of 2D single crystal (G-phase, B-phase).[18a]

1.2.2 Fluorescent optical recording media

The solid-state fluorescence of organic π-conjugated materials strongly relies on the molecular structure and intermolecular interactions by different arrangement. Polymorphism where molecules are arranged in multiple packing modes possess substantially different physical and chemical properties depending on stacking sequence. It has provoked the fundamental investigation for understanding the mechanism of this fascinating phenomenon.[19] In addition, studies on the polymorphism are of importance for a variety of applications in the fields of optoelectronics, such as optical memory and sensors.[20] Recently, fluorescence switching induced by various external stimuli (temperature, vapor and pressure) have been understood by elucidating stacking arrangement in the molecular solids through X-ray diffraction (XRD) study of the individual phase. Our group has intensively focused on the nature of solid state interaction by engineering molecular electronic coupling and secondary intermolecular interactions. Dicyanodistyrylbenzene-based AIEE active DBDCS (See Figure 1.5 (a)) exhibiting two color fluorescence switching with multi-stimuli has been reported. [13b] Interestingly, DBDCS forms fluorescent molecular sheets with stacking and shear-sliding capabilities, which leads to two different phases called as G / B-phase. While the G-phase shows excimeric emission, excitonic interaction is favored in case of B-phase. On the basis of thorough photophysical, structural and computational studies, we identified distinct two phases and demonstrated rewritable fluorescent optical recording media

responding to multi-stimuli quickly (See Figure 1.5 (b), (c)).

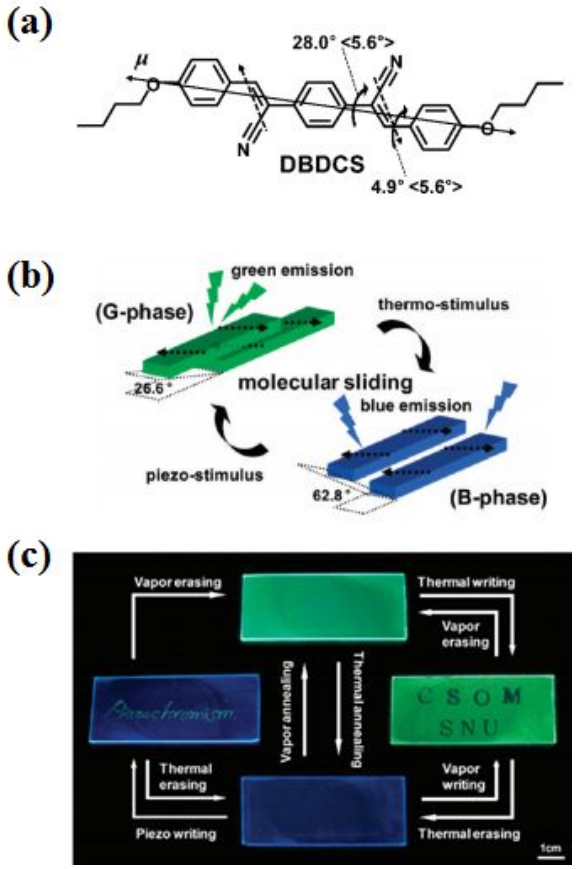

Figure 1.5. (a) Molecular structure of DBDCS and local, transition dipole moments, (b) Illustration of two different modes of slipped stacking in DBDCS molecular sheets, (c) Demonstration of fluorescence writing / erasing.[13b]

1.2.3 Biological imaging

Long term non-invasive cell tracing by using fluorescent image agent has emerged as significant research field in biomedical engineering and life science. Fluorescence technique has advantages of inexpensive, high resolutions at the cellular level and biocompatibility.[21] However, the prevalent organic fluorescent materials exhibit almost no fluorescence in the aqueous environment because of the aggregate formation due to large π-conjugated aromatic rings with hydrophobicity. To avoid the concentration quenching phenomenon, there have been continuous efforts in sophisticated molecular modification for water dispersible or water soluble capability. In this respect, aggregation-induced enhanced emission (AIEE) active materials have attracted considerable attention due to their unique property. Amphiphilic 12EO-CNTFMBE which contains hydrophilic part at the one side of molecule has been reported. This molecule spontaneously forms green fluorescent organic nanorods in water and performs as nanocarrier.[22] Besides, Matsuda group have developed self-assembling amphiphilic fluorescent molecules by utilizing hydrophilic part into the both ends of molecule.[23] CNBE derivative 2 shows AIEE phenomenon in water and detailed mechanism is understood by exhaustive photophysical studies. This facile and effective strategy with enhanced emission property opens up a new way for biological imaging and sensing.

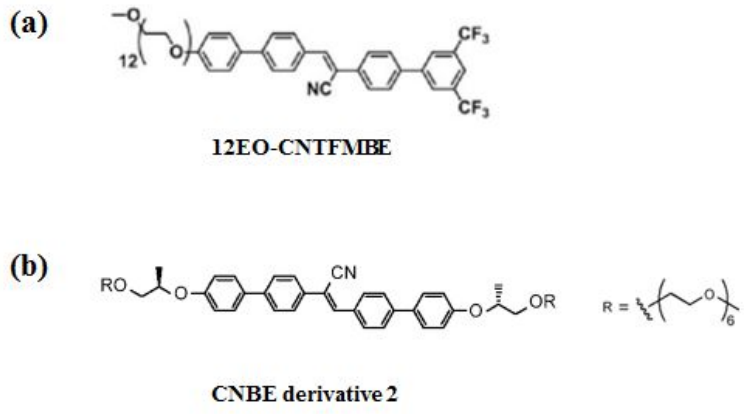

Figure 1.6. (a) Molecular structure of 12EO-CNTFMBE and (b) CNBE derivative 2.

1.3 Characteristics and Significance of Red Fluorophores

Red is one of primary colors that are necessary for practical application such as white lighting and full-color displays. In general, red fluorescence comes from materials with narrow bandgap resulted from attachment of strong donor (D) and acceptor (A) on fluorophores or extensively π-conjugated planar molecules such as porphyrins and polycyclic aromatic hydrocarbon. Among recently reported π-conjugated organic molecules including such structural features, some molecular structures with high photoluminescence quantum yield in the far-red region are as follows (See Scheme 1.2).[24]

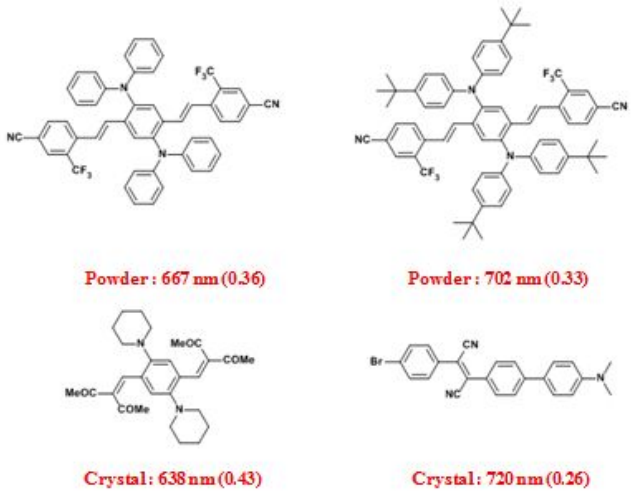

Scheme 1.2. Molecular structure of highly solid-state red emissive materials with emission maximum wavelength and solid-state photoluminescence quantum yield.

Alike other organic π-conjugated molecules, red fluorescent materials usually show strong emission in solution, but become weakly emissive or non-fluorescent in the aggregate state unless J-aggregates are formed. In fact, these fluorophores are prone to form dense aggregate by strong π-π interaction and dipole-dipole interaction and inevitably face fluorescence quenching in the solid state. To resolve this problem, a number of researchers have paid much attention to the development of organic molecules exhibiting highly efficient solid-state red fluorescence by adopting branched and non-planar molecular architecture, J-aggregate formation, cross-dipole stacking, and intramolecular charge transfer transition (ICT). In addition, recently, there has been growing interest in the design of π-conjugated molecules that function in the far-red to near infra-red region motivated by various potential applications in night vision displays, biological imaging, fluorescent molecular sensors, and optical communications.[25]

1.4 Research Objectives

To date, organic π-conjugated materials have attracted tremendous attention because of their versatility in tuning electronic and optical properties, as well as promising potential of diverse optoelectronic devices. Whereas a great number of molecules are known to be strongly fluorescent in dilute solution, most of them usually exhibit decreased fluorescence in solid state. Therefore, design and synthesis of highly solid-state emissive materials is a fundamental and significant research topic for realizing a wide range of applications, such as organic light-emitting field-effect transistors (OLE-FETs), organic lasers, and sensors. In our group, a series of cyanostilbene derivatives exhibiting highly efficient fluorescence in the solid state (powder, nanoparticle, gel) have been reported. The modulated luminescent properties by systematic design have been thoroughly investigated through optical, structural, photophysical experiments.

Herein, we report on the materials design, synthesis, and applications of novel β-dicyanodistyrylbenzene derivatives exhibiting strong solid-state fluorescence in far-red and Near Infra-Red region. We newly designed and synthesized D-A-D-A-D type β-DCS derivatives by integrating various N-amine moieties with strong donating property for bright Near Infra-Red emitters. To explore highly fluorescent characteristics in the solid state, we studied fundamental photophysical, electronic properties and crystal structure by UV-Vis spectroscopy, cyclic voltammetry (CV), and single crystal X-ray analysis.

1.5 Bibliography

1. a) H. Yersin, Highly Efficient OLEDs with Phosphorescent Materials, Wiley-VCH, Weinheim, **2008**; b) R. H. Friend, R. W. Gymer, A. B. Holmes, J. H. Burroughes, R. N. Marks, C. Taliani, D. D. C. Bradley, D. A. Dos Santos, J. L. Bredas, M. Logdlund and W. R. Salaneck, Nature., **1999**, 397, 121.
2. a) U. Scherf, S. Riechel, U. Lemmer and R. F. Mahrt, Curr. Opin. Solid State Mater. Sci., **2001**, 5, 143; b) I. D. W. Samuel and G. A. Turnbull, Chem. Rev., **2007**, 107, 1272.
3. a) O. S. Wolfbeis, J. Mater. Chem., **2005**, 15, 2657; b) S.-W. Zhang and T. M. Swager, J. Am. Chem. Soc., **2003**, 125, 3420.
4. M. Shimizu and T. Hiyama, Chem.-Asian J., **2010**, 5, 1516.
5. Birks, J. B. In Photophysics of Aromatic Molecules, Wiley: London, **1970**.
6. a) J. Luo, Z. Xie, J. W. Y. Lam, L. Cheng, H. Chen, C. Qiu, H. S. Kwok, X. Zhan, Y. Liu, D. Zhu and B. Z. Tang, Chem. Commun., **2001**, 1740; b) B. Z. Tang, X. Zhan, G. Yu, P. P. S. Lee, Y. Liu and D. Zhu, J. Mater. Chem., **2001**, 11, 2974.
7. Y. Dong, J. W. Y. Lam, A. Qin, J. Liu, Z. Li, B. Z. Tang, J. Sun and H. S.

Kwok, Appl. Phys. Lett., **2007**, 91, 011111.

8. J. Chen, C. C. W. Law, J. W. Y. Lam, Y. Dong, S. M. F. Lo, I. D. Williams, Zhu and B. Z. Tang, Chem. Mater., **2003**, 15, 1535.
9. a) B.-K. An, S.-K. Kwon, S.-D. Jung, S. Y. park, J. Am. Chem. Soc., **2002**, 124, 14410; b) J. Gierschner and S. Y. Park, J. Mater. Chem. C, **2013**, 1, 5818.
10. Z. Xie, B. Yang, F. li, G. Cheng, L. Liu, G. Yang, H. Xu, L. Ye. M. Hanif, S. Liu, D. Ma and Y. Ma, J. Am. Chem. Soc., **2005**, 127, 14152.
11. A. Wakamiya, K. Mori and S. Yamaguchi, Angew. Chem., Int. Ed., **2007**, 46, 4273.
12. J. Gierschner, M. Ehni, H.-J. Egelhaaf, B. M. Medina, D. Beljonne, H. Benmansour, G. C. Bazan, J. Chem. Phys., **2005**, 123, 144914.
13. a) B.-K. An, J. Gierschner, S. Y. Park, Acc. Chem. Res., **2011**, 45, 544; b) S.-J. Yoon, J. W. Chung, J. Gierschner, K. S. Kim, M.-G. Choi, D. Kim, S. Y. Park, J. Am. Chem. Soc., **2010**, 132, 13675.
14. Gruszecki, W. I. J. Biol. Phys., **1991**, 18, 99.
15. a) Li, R.; Hu, W.; Liu, Y.; Zhu, D. Acc. Chem. Res., **2010**, 43, 529; b) Jiang, L.; Dong, H.; Hu, W. J. Mater. Chem., **2010**, 20, 4994.
16. H. Koezuka, A. Tsumara and T. Ando, Synth. Met., **1987**, 18, 699.
17. Marta Mas-Torrent and Concepcio´ Rovira, Chem. Soc. Rev., **2008**, 37,

827.

18. a) S. K. Park, J. H. Kim, S.-J. Yoon, O. K. Kwon, B.-K. An, S. Y. Park, Chem. Mater., **2012**, 24, 3263; b) S. K. Park, S. Varghes, J. H. Kim, S.-J. Yoon, O. K. Kwon, B.-K. An, J. Gierschner, S. Y. Park, J. Am. Chem. Soc., **2013**, 135,4757.
19. Anthony, S. P., ChemPlusChem., **2012**, 77, 518.
20. a) Y. Sagara , T. Kato , Nat. Chem., **2009**, 1 , 605; b) A. Pucci , G. Ruggeri , J. Mater. Chem., **2011**, 21 , 8282; c) K. Ariga , T. Mori , J. P. Hill , Adv. Mater., **2012**, 24 , 158.
21. M. F. Kircher, S. S. Gambhir and J. Grimm, Nat. Rev. Clinic. Oncol., **2011**, 8, 677.
22. S. Shin, S. H. Gihm, C. R. Park, S. Kim, S. Y. Park, Chem. Mater., **2013**, 25, 3288.
23. T. Hirose, K. Higashiguchi, K. Matsuda, Chem. Asian J., **2011**, 6, 1057.
24. a) R. Kaki, Y. Takeda, T. Hiyama, N. Nagai, H. Yamagishi, H. Furutani, M. Shimizu, Angew. Chem. Int. Ed., **2012**, 51, 1; b) Y. Takeda, M. Higashi, T. Hiyama, M. Shimizu, Angew. Chem. Int. Ed., **2009**, 48, 3653.
25. a) K. Kiyose, H. Kojima, T. Nagano, Chem. Asian j., **2008**, 3, 506; b) J. O. Escobedo, O. Rusin, S. Lim, R. M. Strongin, Curr. Opin. Chem. Biol., **2010**, 14, 64.

Chapter 2. Synthesis and Characterization of Stimuli-Responsive β-Dicyanodistyrylbenzene Derivatives exhibiting Highly Efficient Solid-state Emission in the Far-red to Near Infra-Red Region

2.1. Design concept and Target materials

There have been great efforts for development of organic π-conjugated small molecules particularly related to their diverse applications in optoelectronics over the past decades. To understand systematic structure-property relationships in the solid state, we have focused on the distyrylbenzene (DSB) derivatives including cyano-vinylene functionality due to extremely large fluorescence enhancement in the solid state (nanoparticle, powder, gel, etc).[1] Through well-defined single crystal analysis of systematically designed DCS derivatives, we have comprehensively studied fundamental solid-state properties such as efficient emission and fluorescence switching based on manipulation of the molecular stacking and demonstrated the potentials of organic field-effect transistors (OFETs) and rewritable fluorescent optical recording media. Recently, we have reported color-tuned dicyanodistyrylbenzene derivatives with spontaneous and stimulated emission characteristics, as well as intense

emission.[2] All the four molecules have strong crystallization tendency assisted by polar donor-acceptor (D-A) functionalities and then their high quality crystals were prepared using slow diffusion method. Among four compounds with different position of cyano functionality and attaching butoxy groups at the periphery or not, β-MODBDCS exhibits pronounced red fluorescence (λ_{max} = 625 nm) and high fluorescence quantum yield (Φ_{FL} = 0.46) (See Figure 2.1).

On the other hand, Weder and coworkers have also developed dicyanodistyrylbenzene derivatives which display piezochrmic fluorescence in the polymer matrix.[3] It was illustrated that different packing polymorphs coexist, resulting in peculiar emission properties. While DCS molecule forms aggregates in the polymer and leads to dominated excimeric emission, fluorescence change occurs from the excimeric to monomer emission by the tensile deformation (See Figure 2.2). This property could be reversibly and repeatedly switched upon external stimuli and tuned via polymer/dye ratio, processing condition. It appears attractive potentional for internal strain sensors in polymer towards technological applications.

On the basis of aforementioned materials, I intended to design and synthesize new dicyanodistyrylbenzene-based derivatives including not only far-red to Near Infra-Red emission but also luminescence switching behavior (See Figure 2.3). I designed D-A-D-A-D type β-DCS molecules due to longer effective π-conjugation length of β-DCS than that of α-DCS in the solid state. Furthermore, we introduced the terminal amine moieties and fixed methoxy substitued core to check the effect of different alkyl chain length and

bulkiness. In this part, I synthesized target materials β-MODEADCS, β-MODBADCS, β-MODBADCS and investigated fundamental thermal, electrochemical, photophysical properties, as well as structural analysis especially focusing on unique highly far-red to Near Infra-Red fluorescence in the solid-state.

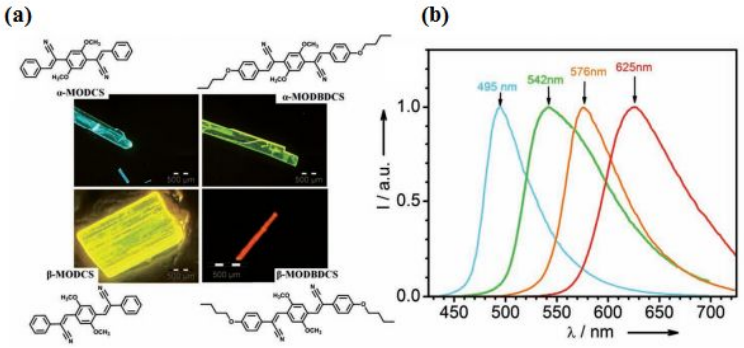

Figure 2.1. (a) Chemical structure of compounds and their crystal images (b) Normalized fluorescence spectra in single crystla at 298K.[2]

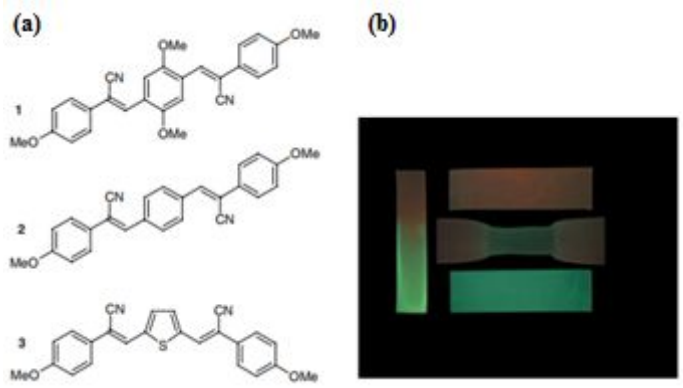

Figure 2.2. (a) Chemical structure of compounds and (b) Optical images (under excitation at 365 nm) of LLDPE blend films comprising **1** in moleculary disperesed (green) and aggregated (red) form.[3]

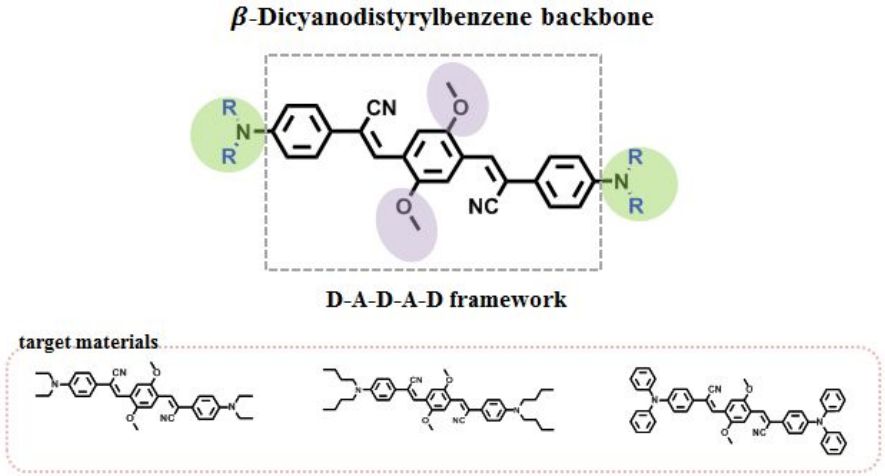

Figure 2.3. The molecular framework and target materials.

2.2. Experimental

2.2.1 Synthesis

β-Dicyanodistyrylbenzene derivatives (β-MODEADCS, β-MODBADCS, β-MODPADCS) were synthesized according to the procedure shown in Scheme 2-1. All chemicals were commercially available and used without purification. Full synthetic details, ^{1}H NMR, mass spectroscopy, and elemental analysis characterizations are found below.

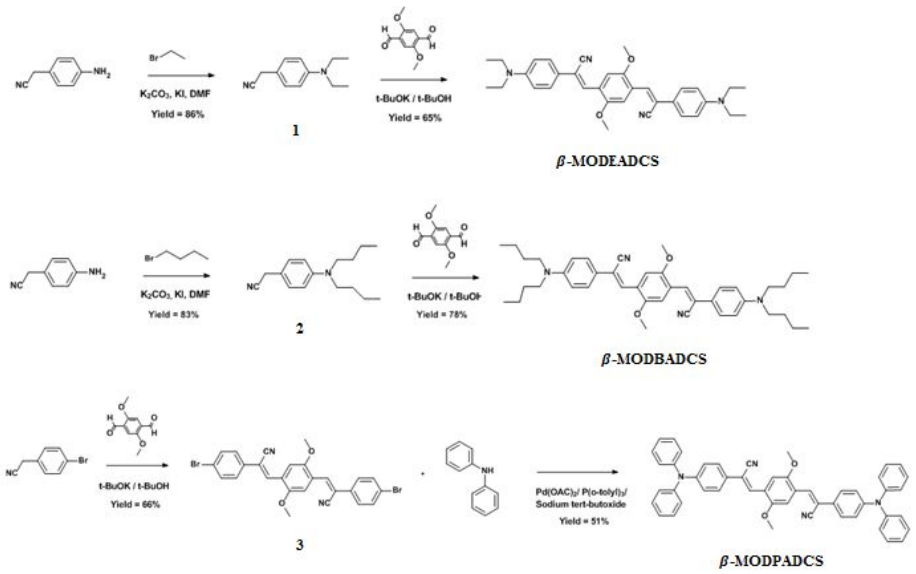

Scheme 2.1. The synthetic schemes of β-MODEADCS, β-MODBADCS, β-MODPADCS.

2-(4-(Diethylamino)phenyl)acetonitrile (1). To a solution of 2-(4-aminophenyl)acetonitrile (2 g, 15.1 mmol) in dry DMF (20ml), were added K_2CO_3 (4.6 g, 33.2 mmol) and KI (catalytic amount) and the mixture was stirred at 80 °C. Bromoethane (2.5ml, 33.3 mmol) was slowly dropped into the mixture. The reaction lasted overmight. After cooling to room temperature, the mixture was poured into brine and extracted with dichloromethane. The organic phase dried over $MgSO_4$ and the solvent was evaporated in vacuo. The product (2.44 g, 86 %) was obtained by column chromatography using ethyl acetate and n-hexane (1:6 v/v). ^{1}H NMR ($CDCl_3$) δ [ppm]: 7.13(d.2H, Ar-H), 6.63(d.2H, Ar-H), 3.60 (d.2H, -CH_2), 3.35(q.4H, CH_2), 1.14(t.6H, -CH_3).

2-(4-(Dibutylamino)phenyl)acetonitrile (2). To a solution of 2-(4-aminophenyl)acetonitrile (2 g, 15.1 mmol) in dry DMF (20ml), were added K_2CO_3 (4.6 g, 33.2 mmol) and KI (catalytic amount) and the mixture was stirred at 80 °C. 1-Bromo-buthane (3.6ml, 33.3 mmol) was slowly dropped into the mixture. The reaction lasted overmight. After cooling to room temperature, the mixture was poured into brine and extracted with dichloromethane. The organic phase dried over $MgSO_4$ and the solvent was evaporated in vacuo. The product (3.07 g, 83 %) was obtained by column chromatography using ethyl acetate and n-hexane (1:8 v/v). ^{1}H NMR ($CDCl_3$) δ [ppm]: 7.10(d.2H, Ar-H), 6.59(d.2H, Ar-H), 3.61(d.4H,-CH_2), 1.55(q.4H, CH_2), 1.33(m.4H,-CH_2), 0.94(t.6H, -CH_3).

(2Z,2'Z)-3,3'-(2,5-dimethoxy-1,4-phenylene)bis(2-(4-(diethylamino) phenyl)acrylonitrile) (β-MODEADCS). The mixture of 2-(4-(diethylamino) phenyl)acetonitrile (1.24 g, 6.6 mmol) and 2,5-dimethoxyterephthalaldehyde (0.64 g, 3.3 mmol) in tert-butyl alcohol (15 ml) was stirred at 50 ^{o}C. Potassium tert-butoxide (0.74 g, 6.6 mmol) powder was dropped into the mixture and stirred for 2 hours. After that, it was quenched with methanol. The resulting precipitate was filtered and purified by column chromatography using dichloromethane and recrystallization from dichloromethane and methanol solution. Red powder of β-MODEADCS (2.3 g, 65 %) was obtained after recrystallization three times in ethanol. ^{1}H NMR ($CDCl_3$) δ [ppm]: 7.87(s.2H,-CH_2), 7.79(s.2H, Ar-H), 7.56(d.4H, Ar-H), 6.70(d. 4H, Ar-H), 3.95(s.6H, -OCH_3), 3.42(q.8H, -CH_2), 1.21(t.12H, -CH_3).

(2Z,2'Z)-3,3'-(2,5-dimethoxy-1,4-phenylene)bis(2-(4-(dibutylamino) phenyl)acrylonitrile) (β-MODBADCS). The mixture of 2-(4-(dibutylamino) phenyl)acetonitrile (1.1 g, 4.9 mmol) and 2,5-dimethoxyterephthalaldehyde (0.57 g, 2.45 mmol) in tert-butyl alcohol (15 ml) was stirred at 50 ^{o}C. Potassium tert-butoxide (0.55 g, 4.9 mmol) powder was dropped into the mixture and stirred for 3 hours. After that, it was quenched with methanol. The resulting precipitate was filtered and purified by column chromatography using dichloromethane and recrystallization from dichloromethane and methanol solution. β-MODEADCS bulk red powder (2.5 g, 78%) was obtained after recrystallization three times in ethanol. ^{1}H NMR ($CDCl_3$) δ [ppm]: 7.87(s.2H,-CH_2), 7.78(s.2H, Ar-H), 7.55(d.4H, Ar-H), 6.67(d. 4H, Ar-

H), 3.93(s.6H, -OCH_3), 3.31(q.8H, -CH_2), 1.55(q.8H, CH_2), 1.37(m.8H, -CH_2), 0.97(t.12H, -CH_3).

(2Z,2'Z)-3,3'-(2,5-dimethoxy-1,4-phenylene)bis(2-(4-bromophenyl) acrylonitrile) (3). The mixture of 2-(4-bromophenyl)acetonitrile (404 mg, 2.0 mmol) and 2,5-dimethoxyterephthalaldehyde (200 mg, 1.0 mmol) in tert-butyl alcohol (40 ml) and tetrahydrofuran (5 ml) was stirred at 50 ^oC. Potassium tert-butoxide (230 mg, 2.0 mmol) powder was dropped into the mixture and stirred for 1 hour. The resulting precipitate was filtered and purified by column chromatography using dichloromethane and recrystallization from dichloromethane and methanol solution. This orange color compound (750 mg, 66 %) was obtained. ^1H NMR ($CDCl_3$) δ [ppm]: 7.88(s.2H,-CH_2), 7.56(d.4H, Ar-H), 7.44(d.4H, Ar-H), 6.70(d.2H, Ar-H), 3.91(s.6H, -OCH_3).

(2Z,2'Z)-3,3'-(2,5-dimethoxy-1,4-phenylene)bis(2-(4-(diphenylamino) phenyl)acrylonitrile) (β-MODPADCS). A single-necked 100-mL round-bottomed flask was charged with the diphenylamine (77 mg, 0.45 mmol) sodium tert-butoxid (44 mg, 0.45 mmol), palladium acetate (5 mg, 0.02 mmol), and dry toluene (20ml), (2Z,2'Z)-3,3'-(2,5-dimethoxy-1,4-phenylene)bis(2-(4-bromophenyl)acrylonitrile) (100 mg, 0.18 mmol) and tri-o-tolylphosphine (10 mg, 0.03 mmol) and heated at 110 ^oC for 24hours under a nitrogen atmosphere. After cooling, the mixture was quenched with water and extracted with ethyl acetate, and then dried over anhydrous Na_2SO_4. β-MODPADCS was purified by column chromatography using dichloromethane

and n-hexane (1:3 v/v). Bulk red powder (510 mg, 51 %) was obtained after recrystallization two times in ethyl acetate. ^{1}H NMR ($CDCl_3$) δ [ppm]: 7.88(s.4H, CH_2, Ar-H), 7.55(d.4H, Ar-H), 7.29(d.8H, Ar-H), 7.10(m.16H,-CH_2), 3.94(s.6H, -OCH_3).

2.2.2 Sample preparation

Nanoparticle suspensions were obtained by following methods. In case of β-MODEADCS and β-MODBADCS, the stock solutions of each material in tetrahydrofuran were prepared with 0.5 mg/mL concentration. The solutions of two materials were injected into one 20 mL volume glass vial and tetrahydrofuran was evaporate using evaporator. After that, they were well-mixed vigorously with vortex mixer. However, β-MODPADCS nanoparticle was fabricated by a simple re-precipitation method from solution in THF (2x 10^{-5} mol L^{-1}) by injection of water (distilled and filtered by membrane filter with 0.2 μm pore size) in 2:98 volume fraction under vigorous stirring.

Single crystal of β-MODEADCS was obtained at room temperature by slow diffusion of methanol vapor into the chlorobenzene.

Powder samples were prepared by recrystallization from hot ethanol solutions as red crystallites.

2.2.3 Spectroscopic Characterization

^{1}H-NMR spectrum was recorded on a Bruker, Avance-300 (300 MHz) in $CDCl_3$ solution. Mass spectra were measured on a JEOL, JMS 600W spectrometer using electron impact (EI) or chemical ionization (CI), and JEOL JMS AX505WA spectrometer using fast atom bombardment (FAB) method. Significant fragments are reported in the following fashion: *m*/*z* (relative intensity). Elemental analysis was carried out using a CE instruments, EA1110 elemental analyzer. UV-visible absorption spectra were recorded on a Shimazu, UV-1650 PC spectrometer. Photoluminescence emission and excitation spectra were obtained using a Photo Technology International, Felix32 QM-4 and a Varian, Cary Eclipse Fluorescence spectrophotometer, correcting the spectra for the sensitivity of the detection system and the characteristics of the lamp, respectively. The absolute photoluminescence quantum efficiencies of the powder and crystal samples were measured using integrating sphere (Labsphere Co., 600 diameter). Relative fluorescence quantum yield was measured using Rhodamine 6G in ethanol as the standard. Time-resolved fluorescence lifetime experiments were performed by the time-correlated single photon counting (TCSPC) technique with a FluoTime200 spectrometer (PicoQuant) equipped with a PicoHarp300 TCSPC board (PicoQuant) and a PMA182 photomultiplier (PicoQuant). The excitation source was a 377 nm picoseconds pulsed diode laser (PicoQuant, LDH375) driven by a PDL800-D driver (PicoQuant) with fwhm ~70 ps. The multi-exponential least square fitting procedure was carried out with the Fluofit

software (PicoQuant), taking into possible double excitations of the IRF within the deconvolution. Energy level was carried out using photoelectron spectrometer AC-2 in Kyeongpook national university.

2.2.4 X-ray and Thermal analysis

A single crystal was collected under ambient condition and crystal data collection was performed using a Bruker SMART APEX2 ULTRA and a APEX II CCD area detector with a multilayer-monochromated Mo Kα radiation (λ = 0.71073 Å) generated by a rotating anode. Cell constants were determined from a list of reflections found by an automated search routine. Data were collected using the full sphere routine and corrected Lorentz and polarization effects. XRD measurements were performed on a Powder X-ray Diffractometry (D8-Advance, Bruker, Germany), operating at 3kW. Differential scanning calorimetry (DSC) was performed on a Perkin Elmer DSC7 with a heating rate of $10^{o}C\ min^{-1}$.

2.2.5 Quantum chemical calculation

Single molecule calculations were performed at the density functional theory (DFT) level of theory with the Gaussian09 software. Herein, the ground state geometry in the gas phase was fully optimized using B3LYP functional and 6-31G** basis set.

2.3. Results and Discussion

2.3.1 Optical properties in various phases

The molecular structure of target materials (β-MODEADCS, β-MODBADCS, β-MODPADCS) is depicted and intense red fluorescence images of each powder are shown in Figure 2.4. To understand the origin of the intriguing photophysical properties in the solid state, we preferentially determined the solution property of β-MODCS series and their overall photoluminescence data are summarized in Table 2.1. Figure 2.5 (a) shows the absorption and emission spectra in tetrahydrofuran solution, which have little difference in three target materials' spectral shape and maximum wavelength (λ_{abs}, λ_{em}). These results are attributable to their structural similarity except for terminal amine substituents. Like other β-DCS based compounds, three target materials also exhibit strong fluorescence (using Rhodamine 6G in ethanol as the standard relative quantum yield Φ_{FL} = 0.88, 0.86, 0.83, respectively). On the other hand, upon addition of water, molecules form aggregated nanostructure shown in spectra of Figure 2.5 (b). While nanoparticle suspensions of β-MODEADCS, β-MODBADCS show blue-shifted absorption from the solution because of formation of H-aggregate assisted by linear molecular structure, absorption maximum wavelength of β-MODPADCS containing relatively less planr phenyl ring is red-shifted slightly. However, in emission spectra, all compounds are red-shifted compared to the

observations in solution. It implies that increase in the effective π-conjugation length occurs through the aggregation-induced planarization of molecular backbone distorted in the isolated state.[4] It is notable that β-MODEADCS exhibits Near Infra-Red fluorescence (λ_{em} = 725 nm), but, relative quantum yield is drastically reduced due to light scattering. Furthermore, we also studied photophysical and stuctural characteristics of powder state. Their emission maximum wavelengths are observed in far-red to Near Infra-Red region with high quantum efficiency (See Table 2.1 and Figure 2. 5 (c)). To verify the highly emissive optical property, we decided to look into the molecular stacking arrangement in the powder state. β-MODBADCS shows typical lamellar structure by observation of obvious (100), (200) peak and β-MODEADCS has crystallinity into the other different direction because it has other peaks besides (100), (200) peaks. In case of β-MODPADCS, very weak diffraction peak is exhibited as we expected, contributed by the effect of bulky phenyl ring at the termini.

The photophysical properties of β-MODEADCS‘s each state are summarized in Table 2.2. As shown Figure 2.7 (a), β-MODEADCS single crystal shows slightly red-shifted emission mawmum wavelength (λ_{em} = 718 nm) in comparison with powder state. Its pretty good fluorescence efficieny is illustated by fluorescent decay profiles (See Fiugure 2.7 (b)). While both nanoparticles and crystal exhibits similar radiative rate constants about k_r = = 2×10^7 s^{-1}, almost four times larger non-radiative rate constant of nanoparticles is observed. Threrfore, aforementioned nanoparticles weak fluorescence is well explained by polycrystallinity of nanoparticle samples

along with a large surface area, so that sequential structural dislocations become trapping sites for the initially generated exciton and increase non-radiative pathway.[5a] Because single crystal's trap concetration is low due to the absence of structural dislocations and contaminations, β-MODEADCS single crystal show relatively low non-radiative rate constant, thereby rendering high quantum effeciency (Φ_{FL} = 0.36). It is fascinating result that β-MODEADCS achieves realization of Near Infra-Red emission as well as efficient fluorescence efficiency among recently reported far-red fluorescent materials.

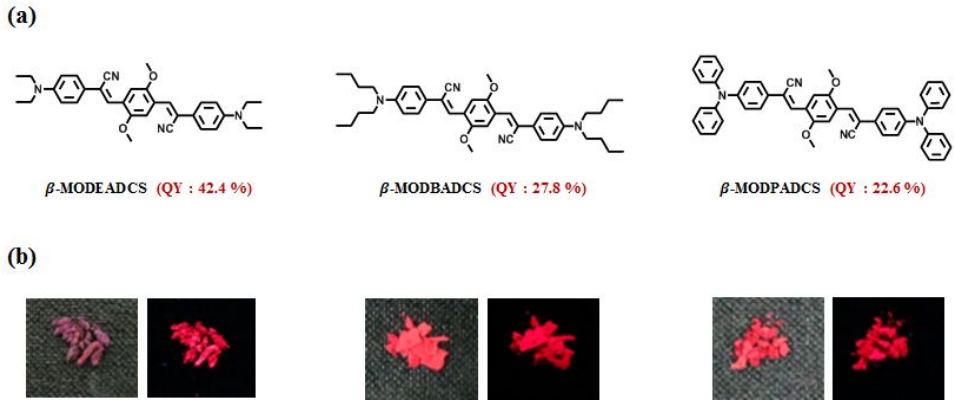

Figure 2.4. (a) The molecular structure and fluorescence quantum yield (Φ_{FL}) of β-MODCS series in powder state, (b) Powder images under room light and UV light.

Table 2.1. Optical properties of β-MODCS series in solution and the solid state; absorption (λ_{abs}) and emission (λ_{em}) wavelength, quantum yields (Φ_{FL}).

	β-MODEADCS	β-MODBADCS	β-MODPADCS
solution			
λ_{abs} [nm]	485	487	472
λ_{em} [nm]	591	591	601
Φ_{FL}	0.88	0.86	0.83
nanoparticles			
λ_{abs} [nm]	460	450	482
λ_{em} [nm]	725	688	662
powder			
λ_{em} [nm]	711	679	676
Φ_{FL}	0.42	0.28	0.23

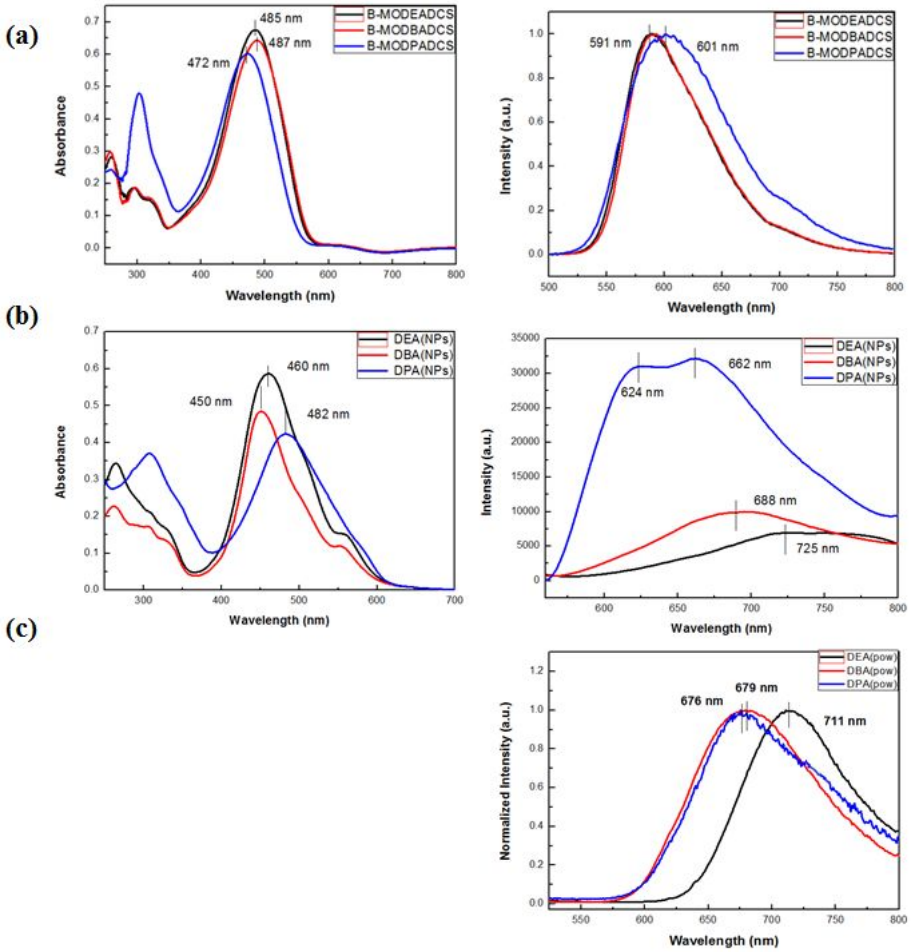

Figure 2.5. (a) UV-Visible absorption and photoluminescence spectra of β-MODCS series in THF solution ($c = 2 \times 10^{-5}$ mol L^{-1}), (b) THF/water mixture ($c = 2 \times 10^{-5}$ mol L^{-1}), (c) Powder.

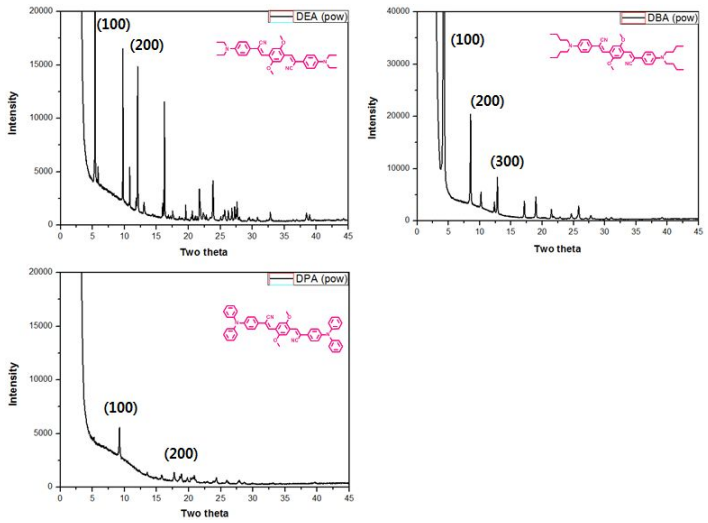

Figure 2.6. XRD patterns of β-MODCS series in powder state.

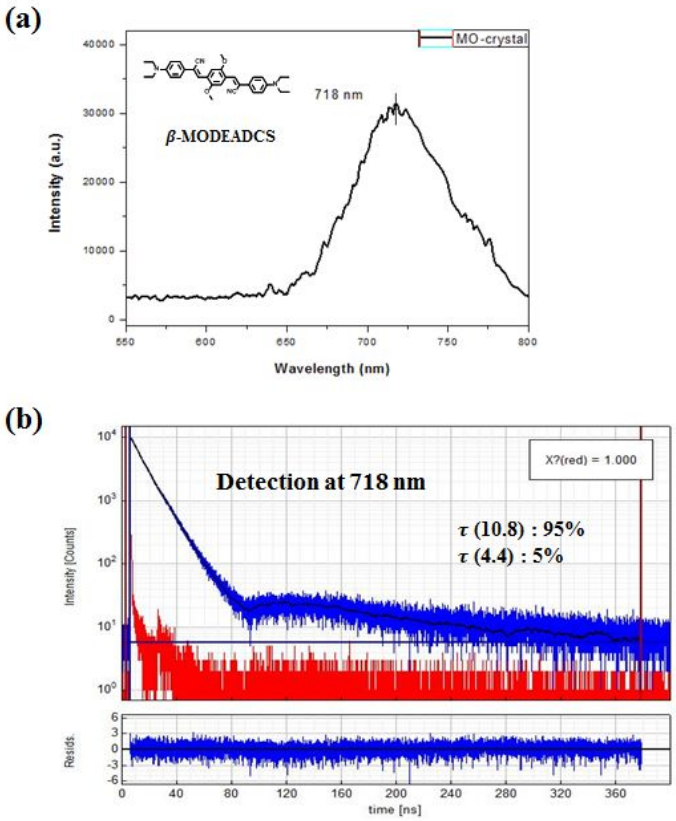

Figure 2.7. (a) Photoluminescence spectra of β-MODCS single crystal, (b) Fluorescence decay profiles of the β-MODCS single crystal (blue line) collected at 730 nm and IRF (red line). Black line shows the fitting curve and lower line shows the residual.

Table 2.2. Photophysical properties of β-MODEADCS.

	Solution	NPs	Pristine powder	Ground powder	crystal
λ_{em} [nm]	591	725	711	656	718
Φ_{FL}	0.88	0.06	0.42	0.34	0.36
τ_F [ns]	2.30	3.27	6.86	1.78	10.2
$k_r / 10^7$ [s^{-1}]	38.3	1.83	6.10	19.1	3.5
$k_{nr} / 10^7$ [s^{-1}]	5.18	28.8	8.50	37.1	6.3

Calculated by $k_r = \Phi_{FL} / \tau_F$, $\tau_F^{-1} = k_r + k_{nr}$

2.3.2 Single crystal analysis of β-MODEADCS

For more precise understanding of intense Near Infra-Red characteristic, single crystal structure was analyzed. As previously described, the pure β-MODEADCS single crystals were obtained by slow diffusion of methanol vapor into the chlorobenzene solution of β-MODEADCS. The molecular stacking structure of Near Infra-Red fluorescent single crystal is depicted in Figure 2.8. β-MODEADCS crystallizes in the triclinic space group P-1 (see Table 2.3) with Z = 1. β-MODEADCS shows similar structure compared to that of β-MODBDCS owing to the similar D-A-D-A-D motif where substituted phenyl rings and cyano-vinylene units serve as donor (D) and acceptor (A), respectively.[2] It is clearly shown that molecules are arranged in slipped π-stacking along the longer molecular axis with pitch angle of 47° which is larger than that of β-MODBDCS and slightly increased interlayer distance of 3.5 Å between molecules compared to 3.34 Å of β-MODBDCS (See Figure 2.8).[2] It was also found that molecules build up a network overall assisted by C-H···O, C-H···π, and C-H···H-C three types of secondary interactions between neighboring molecules. As a result, molecules are densely packed because of strong π-π interactions by the planarization (See Figure 2.9). Significant π-π interactions are usually observed in H-type aggregates, leading to considerable intermolecular vibronic coupling and excimeric emission behavior.[5b] Despite H-aggregation, the emission with excellent quantum yield (Φ_{FL} = 0.36) in Near Infra-Red region is attributed to the relatively weak H-aggregation in comparision with

β-MODBDCS; 1) more substantial x-slip through calculation of pitch angle, and 2) somewhat increased inter-plane distance more than 3.34 Å of β-MODBDCS. In addition, through crystal lifetime measurement (See Table 2. 2), k_r value (2.0 x 10^7 s^{-1}) of β-MODEADCS is similar to β-MODBDCS (1.9 x 10^7 s^{-1}) resulting from a low internal conversion rate and low trap concentrations in the single crystal, so that the radiative process is still a major excited state deactivation pathway. It should be noted that the emission maximum wavelength (λ_{max} = 718 nm) of β-MODEADCS crystal exhibits pronounced red-shift compared to that of β-MODBDCS (λ_{max} = 625 nm).[2] Because there is little difference in structural characteristics through studying single crystal analysis, this largely shifted strong emission indicates that substitution of termial butoxy group with diethylamine endows stronger electron donating property. Also, the large Stokes shift also contributes to intense solid-state fluorescence because of reduced self absorption. Thus, fine tuning of intermolecular interaction by precise molecular design is meaningful approach to control the fluorescent characteristics of functional organic π-conjugated solids.

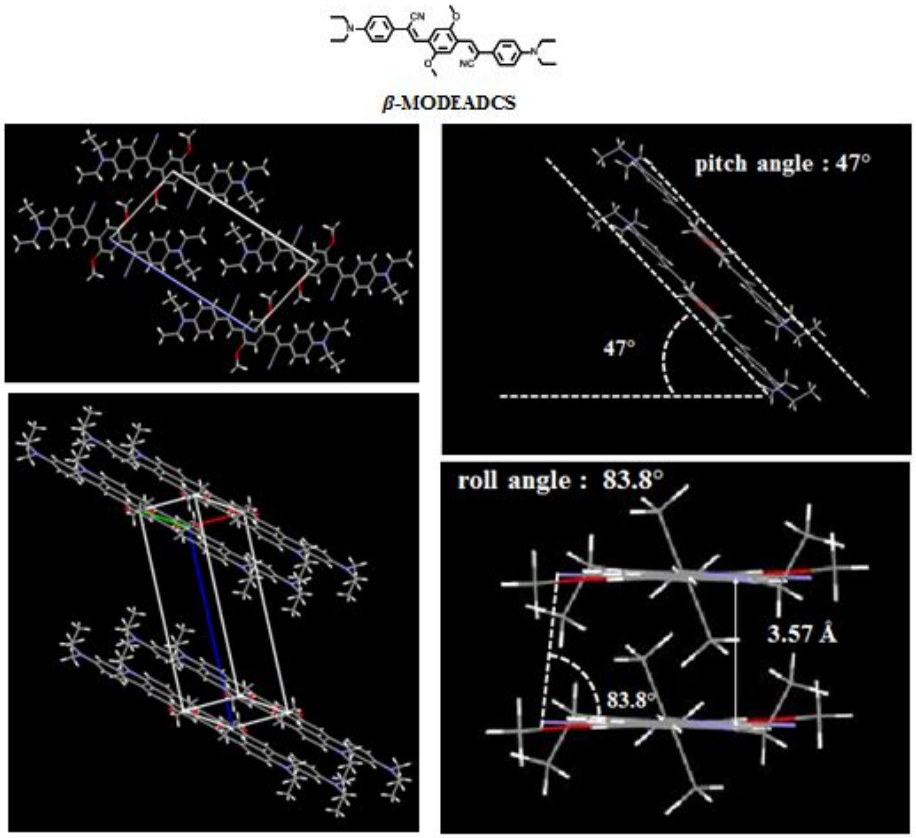

Figure 2.8. β-MODEADCS: molecular structure, crystal packing diagram with a unit cell, pitch angle and roll angle in the single crystal.

Table 2.3. Crystallographic data of β-MODEADCS single crystal.

Identification code	bmodeadcs.	
Empirical formula	C34 H38 N4 O2.	
Formula weight	534.68.	
Temperature	173(2) K.	
Wavelength	0.71073 Å.	
Crystal system	Triclinic	
Space group	P-1.	
Unit cell dimensions	a = 4.7039(2) Å	α= 100.068(2)°.
	b = 9.3029(3) Å	β= 92.587(2)°.
	c = 16.8491(6) Å	γ = 99.396(2)°.
Volume	714.16(5) Å^3.	
Z	1	
Density (calculated)	1.243 Mg/m^3.	
Absorption coefficient	0.078 mm^{-1}.	
F(000)	286.	
Crystal size	0.33 x 0.27 x 0.10 mm^3.	
Theta range for data collection	1.23 to 28.45°.	
Index ranges	-6<=h<=6, -12<=k<=12, -22<=l<=22.	
Reflections collected	19580.	
Independent reflections	3574 [R(int) = 0.0305].	
Completeness to theta = 28.45°	99.2 % .	
Absorption correction	Multi-scan SADABS.	
Max. and min. transmission	0.9921 and 0.9749.	
Refinement method	Full-matrix least-squares on F^2.	
Data / restraints / parameters	3574 / 0 / 181.	
Goodness-of-fit on F^2	1.045.	
Final R indices [I>2sigma(I)]	R1 = 0.0538, wR2 = 0.1601.	
R indices (all data)	R1 = 0.0656, wR2 = 0.1712.	
Largest diff. peak and hole	0.302 and -0.271 e.Å^{-3}	

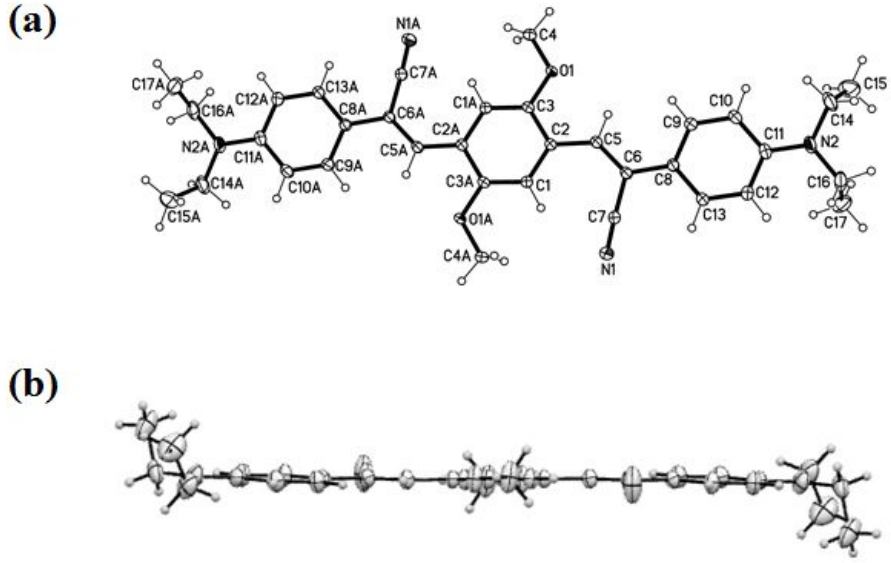

Figure 2.9. ORTEP drawing of β-MODEADCS single crystal. (a) top view, (b) side view.

2.3.3 Luminescence switching by Mechanical and Thermal stimuli

Stimuli-responsive luminescent materials exhibiting change in emission wavelength have attracted considerable attention because of their potential applications such as sensors, switches, and memories.[6] Upon external stimuli, the molecular packing of materials could be dynamically changed between different polymorph states, thereby resulting in distinct switched fluorescence. To date, a number of organic materials responding to solvent vapor,[7] light,[8] and shear force[9] have been developed and applied as candidates for aforementioned applications. Recently, novel piezochromic materials showing high contrast emission switching by precise controlling molecular arrangements have been explored. Among such materials, we have reported donor-acceptor-donor (D-A-D) red fluorescent (λ_{max} = 600 nm) triad, m-BHCDS 1 based on β-dicyanodistyrylbenzene with reversible luminescence on-off switching with high contrast ratio (ca. 10^3).[10]

In an effort to realize luminescence switching in the far-red to Near Infra-Red region, we utilized β-MODEADCS. We prepared pristine powder on the quartz and then applied shear force to the sample using spatula. Interestingly, it was observed that ground state exhibited obviously different intense red fluorescence (Φ_{FL} = 0.34) from the Near Infra-Red emission (Φ_{FL} = 0.42) of the pristine powder and this change in emission was also reversibly returned to original state upon heating process. As shown Figure 2.10, whereas pristine β-MODEADCS showed Near Infra-Red fluorescence with λ_{max} = 711 nm, the maxium emission wavelength of ground powder was largely blue-shifted λ_{max}

= 656 nm. Because it can be expected that mechanical force applied materials usually possess amorphous nature, we studied the packing structure of individual state by powder X-ray diffraction (XRD). The powder XRD pattern of pristine powder showed intense and sharp peaks (See Figure 2.11 (a)) consistent with the simulated peaks from the single crystal data indicating the crystalline phase of the samples. In contrast, the ground powder showed very weak and broad diffraction signal intensity, which implied that a great portion was amorphous phase and very small peaks were remaining crystalline phase after grinding (See Figure 2.11 (b)).[11] These are attributed to the different molecular packing in the solid state by conformational change and degree of π-π overlap by local dipole and various secondary bonding interactions. It can be concluded that crystalline phase including larger overlap and planar structure induces delocalization of excited state and more red-shifted emission supported by single crystal analysis. The shorter wavelength emission of ground sample is originating from the reduced π-overlap and weakened π-π interaction by separated structures. Before verifying the reversibility of the ground sample, we studied their thermal properties by differential scanning calorimetry (DSC). For DSC curve of β-MODEADCS pristine powder (See Figure 2.12 (a)), it showed small endothermic peak at 225 ^{o}C and melting peak at 259 ^{o}C. Ground powder, however, exhibited small peak 197 ^{o}C and melting peak at 257^{o}C during first cycle. In the second cycle, small peak appeared at 229 ^{o}C corresponds to pristine powder and melting peak was constant. Furthermore, ground powder DCS curves firstly showed an exothermic recrystallization peak at relatively lower temperature (69 ^{o}C) (See

Figure 2.12 (b)). These DSC results indicated that the shear force could convert thermodynamically stable crystal to metastable state, which restored into the original crystalline states by exothermic recrystallization process. Therefore, we investigated the optical and structural properties after heating to confirm the reversibility of piezochromic phenomenon. In Figure 2.11 (b), the spectra of the sample subjected to heat treatment at 95 ^{o}C and cooling exhibited sharp diffraction peak again. Also, emission maximum wavelength was red-shifted from 656 nm to 710 nm. These stimuli-responsive luminescence switching was demonstrated in Figure 2.13.

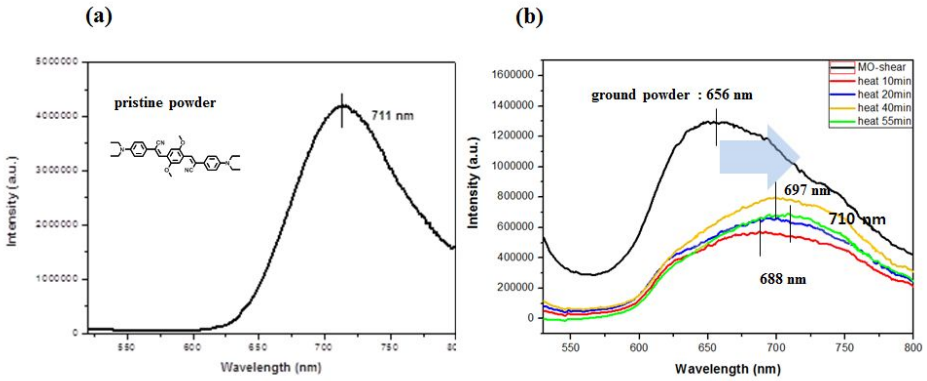

Figure 2.10. (a) Photoluminescence spectra of β-MODEADCS pristine powder, (b) Ground and heated powder.

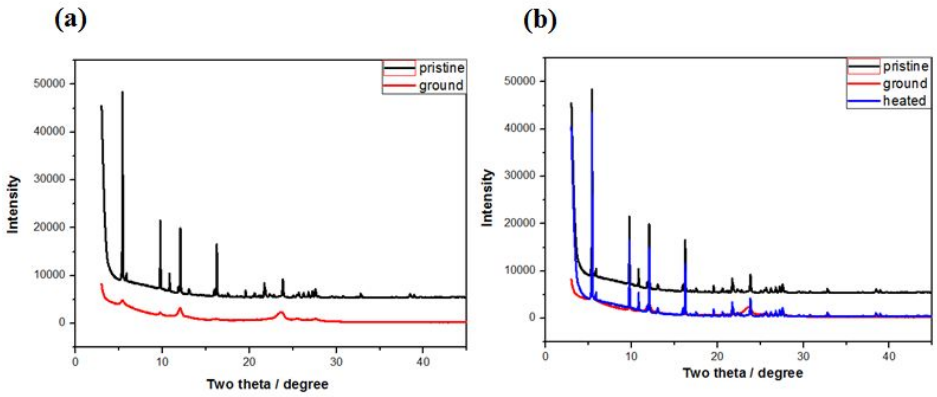

Figure 2.11. (a) Powder XRD patterns of β-MODEADCS pristine and ground powder, (b) Additional powder XRD patterns of heated ground powder.

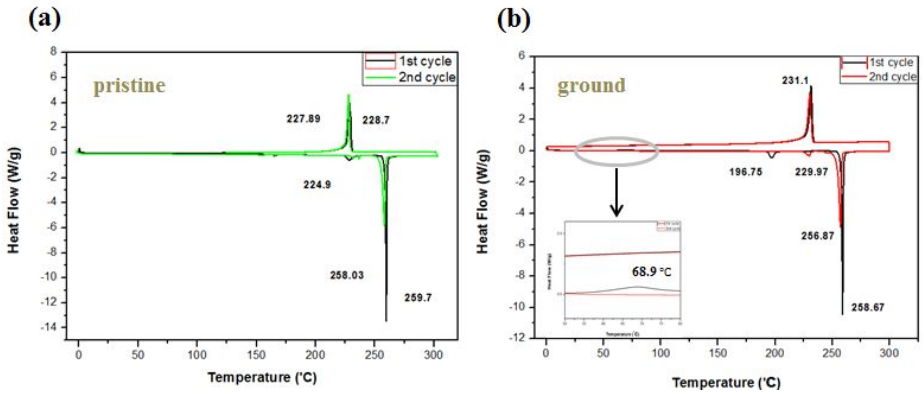

Figure 2.12. (a) DSC curves of pristine powder β-MODEADCS and (b) Ground powder β-MODEADCS.

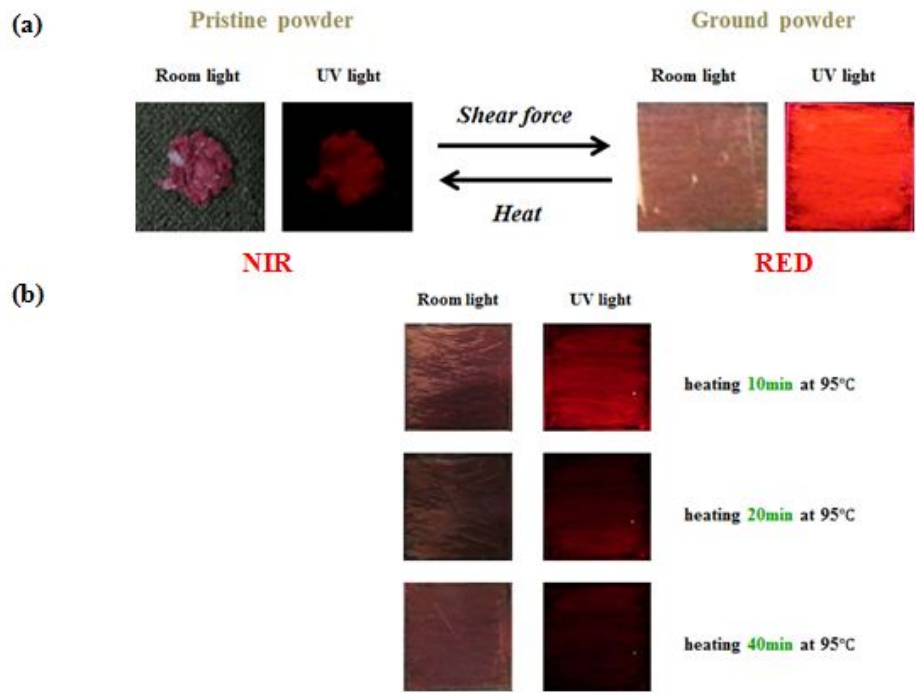

Figure 2.13. (a) Images of pristine powder and ground powder of β-MODEADCS under room light and UV light, (b) Images of fluorescence switching to the original state by heating .

2.3.4 Fabrication and Measurement of SC-OFETs

Research of high-performance p- and n-type organic π-conjugated semiconducting materials is essential for practical applications such as photovoltaic cells, organic logic gates and complementary circuits.[12] There have been steady attention and development of p-type semiconducting materials, for example, rubrene,[13] pentacene,[14] and poly (3-hexylthiophene) (P3HT)[15] showing comparable device properties to that of amorphous silicon. Furthermore, n-type organic semiconducting materials with high electron carrier mobility (μ_e) and elctrochemical stability also have been developed recently. Before device fabrication, SiO_2/Si (300 nm-thick SiO_2) substrates were rinsed by sonication in acetone and iso-propyl alcohol. Then the substrates were exposed to UV (360 nm) for 10 minutes. For the device using crystal, we grew β-MODEADCS crystal on the substrate by dropcasting. We observed flat and 2-dimensional crystal grow well on the substrate treated with SiO_2 by a simple slow solvent evaporation of β-MODEADCS solution, confirmed by optical microscopy (See Figure 2.14 (b)). Among synthesized compounds, it was found that β-MODEADCS exhibits the highest crystallinity owing to the well-balanced intermolecular interactions. It should be noted, however, that the careful balancing between cyano substituted oligo-(p-phenylenevinylene) (OPV) backbones and electron-donating amine units for appropriate energy level is required. DFT calculation of the highest occupied molecular orbital (HOMO) level and the lowest occupied molecular orbital (LUMO) level of β-MODEADCS is

presented in Figure 2.14 (a)). Electrons in HOMO level are distributed throughout the molecular backbone and typical quinoidal structure is observed in LUMO level. The data of energy level by the ultraviolet photoelectron spectroscopy (UPS) measurement has little difference, which is appropriate energy level for p-type transistor device application. Therefore, we fabricated single crystalline p-type field-effect transistor and β-MODEADCS single crystal OFET devices show moderate hole mobility of 0.07 $cm^2V^{-1}s^{-1}$ (See Figure 2.15). All electrical characteristics of devices were measured using a Keithley 4200 semiconductor parameter analyser connected to a probe station in a nitrogen-filled glove box. Through device fabrication, it is expected that introduction of proper functionalities with strong electron-donating property improves the performance of p-type OFETs.

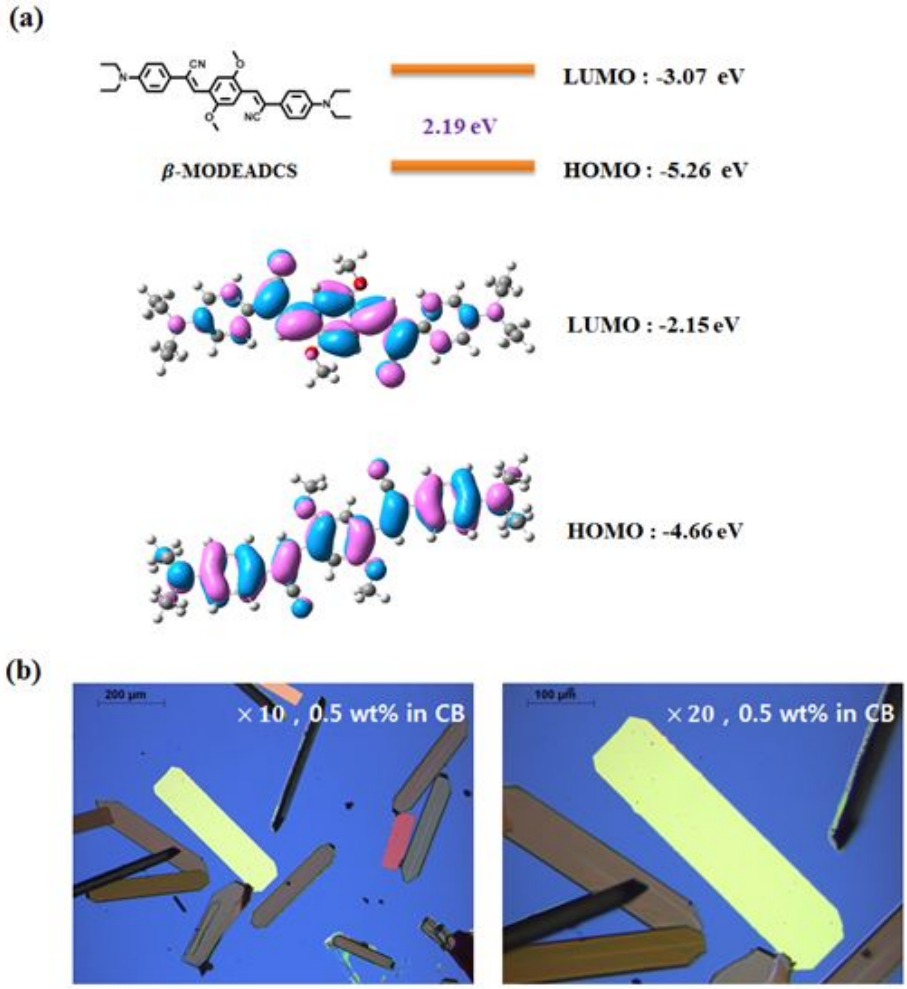

Figure 2.14. (a) Diagram for energy level and electron distributions (LUMO and HOMO) of β-MODEADCS, (b) Optical microscopy image of β-MODEADCS dropcasting.

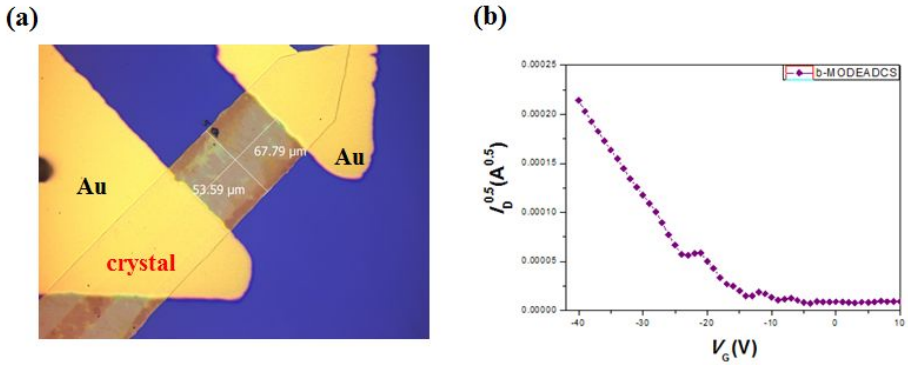

Figure 2.15. (a) Crystal device structure and (b) Output and transfer characteristics of β-MODEADCS single crystal.

2.4. Conclusion

In summary, we have developed β-MODCS series (β-MODEADCS, β-MODBADCS, β-MODPADCS) as novel materials showing efficient solid-state emission in the region of far-red to Near Infra-Red. The quantum yields in the powder state of all compounds are good to high, these emission properties are ascribed to their structural features induced by different aggregation, which are investigated by powder XRD analysis. In particular, powder state of β-MODEADCS emission maximum wavelength is located at λ_{max} = 711 nm with the highest quantum yield of 0.42. Furthermore, β-MODEADCS organizes to form 2-dimensional fine single crystal with regular stacking arrangement by various secondary interaction such as C-H···O, C-H···π, and C-H···H-C interaction between adjacent molecules. Interestingly, β-MODEADCS shows reversible fluorescence switching from Near Infra-Red to red region by mechanical and thermal stimuli. Taking advantage of high crystallinity, we fabricated single crystal p-type OFETs.

These solid-state Near Infra-Red fluorescent materials that do not suffer from concentration quenching are valuable for potential applications in night vision devices, bioimaging, and optical communications.

2.5 Bibliography

1. J. Gierschner and S. Y. Park, J. Mater. Chem. C, **2013**, 1, 5818.
2. S.-J. Yoon, S. Varghese, S. K. Park, R. Wannemacher, J. Gierschner, S. Y. Park, Adv. Optical Mater., **2013**, 1, 232.
3. a) C. Lowe and C. Weder, Adv. Mater., **2002**, 14, 1625; b) B. R. Crenshaw, C. Weder, Chem. Mater., **2003**, 15, 4717.
4. a) H. Bassler, B. Schweitzer, Acc. Chem. Res., **1999**, 32, 173; b) K.. Pichler, D. A. Halliday, D. D. C. Bradley, P. L. Burn, R. H. Friend, A. B. Holmes, J. Phys. Condens. Matter., **1993**, 5, 7155.
5. a) J. Gierschner, L. Luer, B. Milian-Medina, D. Oelkrug, H-J. Egelhaaf, J. Phys. Chem. Lett., **2013**, 4, 2686; b) J. Gierschner, H.-G. Mack, D. Oelkrug, I. Waldner, H. Rau, J. Phys. Chem. A, **2004**, 108, 257.
6. a) Y.-C. Chang, S.-L. Wang, J. Am. Chem. Soc., **2012**, 134, 9848; b) Z. Zhang, D. Yao, T. Zhou, H. Zhang, Y. Wang, Chem. Commun., **2011**, 47, 7782; c) X. Zhang, Z. Chi, Y. Zhang, S. Liu and J. Xu, J. Mater. Chem. C, **2013**, 1, 3376.
7. T. Zhou, T. Jia, S. Zhao, J. Guo, H. Zhang, Y. Wang, Crysta. GrowthDes., **2012**, 12, 179.
8. J. W. Chung, Y. You, H. S. Huh, B.-K. An, S.-J. Yoon, S. H. Kim, S. W.

Lee, S. Y. Park, J. Am. Chem. Soc., **2009**, 131, 8163.

9. a) Y. Sagara, T. Kato, Nat. Chem., **2009**, 1, 605; b) X. Luo, J. Li, C. Li, L. Heng, Y. Q. Dong, Z. Liu, Z. Bo, B. Z. Tang, Adv. Mater., **2011**, 23, 3261.
10. M. S. Kwon, J. Gierschner, S.-J. Yoon, S. Y. Park, Adv. Mater., **2012**, 24, 5487.
11. Z. Zhang, D. Yao, T. Zhou, H. Zhang, Y. Wang, Chem. Commun., **2011**, 47, 7782.
12. a) J. C. Ribierre, T. Fujihara, S. Watanabe, M. Maysumoto, T. Moto, A. Nakao, T. Aoyama, Adv. Mater., **2010**, 22, 1722; b) J. Y. Kim, K. Lee, N. E. Coates, D. Moses, T.-Q. Nguyen, M. Dante, A.
13. N. Stingelin-Stutzmann, E. Smith, H. Wondergem, C. Tanase, P. Blom, P. Smith, D. D. Leeuw, Nat. Mater., **2005**, 4, 601.
14. S. Lee, B. Koo, J. Shin, E. Lee, H. Park, H. Kim, Appl. Phys. Lett., **2006**, 88, 162109.
15. Y. Fu, C. Lin, F.-Y. Tsai, Org. Electron., **2009**, 10, 883.

Chapter 3. Novel Far-Red Fluorescent Molecules forming Self-assembled Nanostructure in Aqueous Systems: Introducing Ethylene oxide Groups to the β-DCS Core

3.1 Design concept and Target materials

Organic materials forming self-assembled structure have attracted considerable research interests due to the capability of controlling nanostructures with distinctive physicochemical properties. Various self-assembly induced structures of amphiphilic molecules are fundamentally investigated in supramolecular chemistry and utilized in bio applications. Among amphiphilic molecular building blocks, rigid-flexible block molecules composed of hydrophobic π-conjugated rod segment and hydrophilic poly(ethylene glycol) (PEG) coil segments are a representative framework, which builds up assemblies spontaneously depending on the appropriate balance between each part.[1] On the basis of molecular design principle, our group reported new fluorinated and PEGlayted α-cyanostilbene type block amphiphile (12EO-CNTFMBE) that can self-assemble into small-dimension, small-aspect-ratio nanorods with aggregation-induced enhanced fluorescence in aqueous environment.[2] However, fluorescence in blue-green region of

12EO-CNTFMBE is undesirable in biological applications because short-wavelength excitation leads to severe damage to cell.

In this research, we newly designed and synthesized β-dicyanodistyrylbenzene-based β-EODEADCS and β-wedge DEADCS, considering greenish-blue fluorescence of 12EO-CNTFMBE in water. We maintained the principal molecular D-A-D-A-D framework shown in Chapter 2 because β-dicyanodistyrylbenzene derivatives exhibit intense far-red to Near Infra-Red emission by introducing N-amine moieties at the termini (See Figure 3.2). In addition, we determined to attach hydrophilic parts into the core vertically instead of adhesion to the one side of molecule and expected that this target material shows different fundamental properties and diverse supramolecular architectures. Therefore, we investigated following points, 1) self-assembly capability in aqueous system with the aid of ethylene oxide group at the core in opposition to encapsulated nanoparticles formation of β-MODEADCS 2) strong Far-red fluorescence in the solid state 3) morphology of self-assembled nanostructures in aqueous system 4) potential as red fluorescent probe for biological imaging.

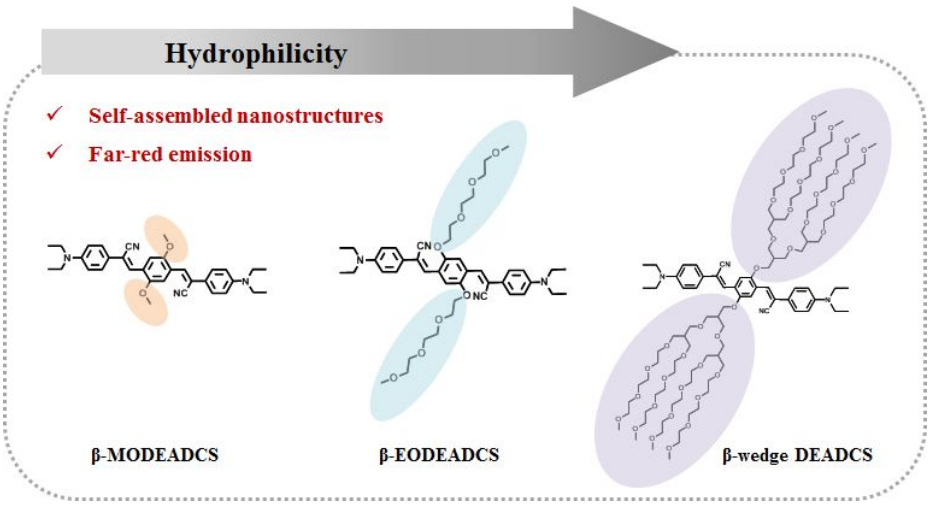

Figure 3.1. The molecular structure of β-EODEADCS and β-wedge DEADCS.

3.2 Experimental

3.2.1 Synthesis

β-EODEADCS was synthesized deprotection, tosylation, alkylation, and Knovenagel condensation according to the procedure shown in Scheme 3-1. All chemicals were purchased commercially, and used without purification. Full synthetic details, ^{1}H NMR, mass spectroscopy, and elemental analysis characterizations are found below.

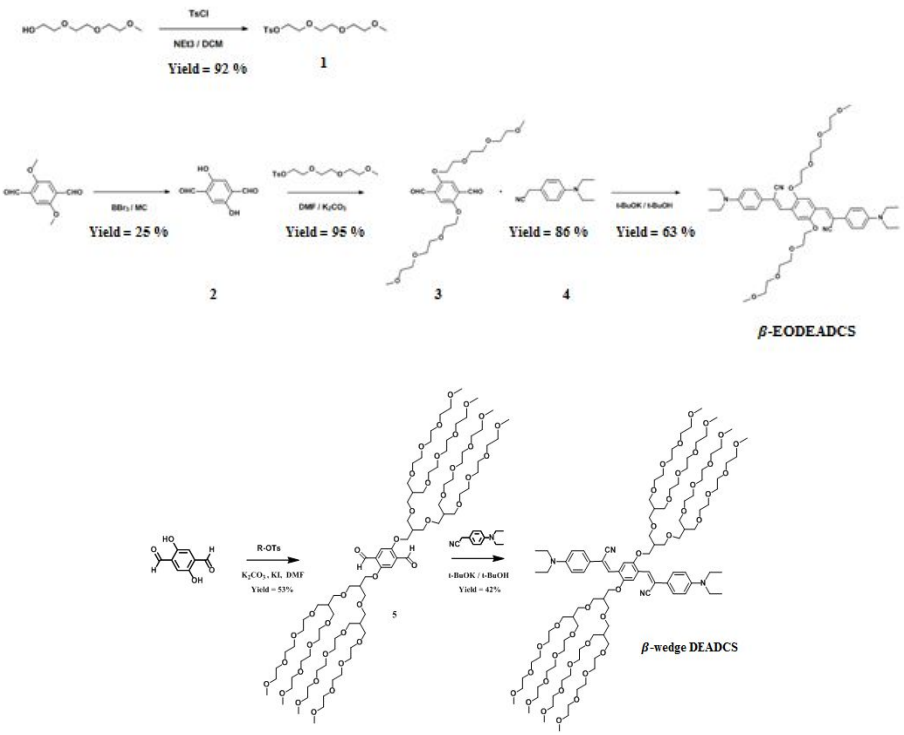

Scheme 3.1. The synthetic scheme of β-EODEADCS and β-wedge DEADCS.

2-(2-(2-methoxyethoxy)ethoxy)ethyl 4-methylbenzenesulfonate (1). The mixture of 2-(2-(2-methoxyethoxy)ethoxy)ethan-1-ol (4 g, 24 mmol) and triethylamine (3.7 g, 37 mmol) in dichloromethane (50 ml) was stirred. 4-methylbenzenesulfonyl chloride (6.04 g, 32 mmol) was put into the solution and stirred for 24 hours at room temperature. After reaction ended, washing with $NaHCO_3$ and drying with $MgSO_4$. Purification was conducted using ethanol and ethyl acetate (1:5 v/v) and oil type product (7.1 g, 92 %) was obtained. ^{1}H NMR ($CDCl_3$) δ [ppm]: 7.75(d.2H, Ar-H), 7.45(d.2H, Ar-H), 3.52-3.7(m.12H, -OCH_2), 3.42(s.3H, -OCH_3), 2.49(s.3H, -CH_3).

2,5-Dihydroxyterephthalaldehyde (2). A solution of 2,5-Dimethoxy terephthalaldehyde (2.00 g, 10.3 mmol) dissolved in a mixture of glacial acetic acid (100 ml) and hydrobromic acid (48%, 80 ml) was refluxed for 7 hours and evaporated to dryness with a rotary evaporator. The recrystallization of the residue from benzene gave the needle-like orange crystals of the desired compound (0.492 g, 25.1%). ^{1}H NMR ($CDCl_3$) δ [ppm]: 10.93 (s, 2H, OH), 9.81 (s.2H,CHO), 7.45 (s.2H, Ar-H).

2,5-bis(2-(2-(2-methoxyethoxy)ethoxy)ethoxy)terephthalaldehyde (3). Put 2,5-dihydroxyterephthalaldehyde (130 mg, 0.78 mmol), 2-(2-(2-methoxyethoxy)ethoxy)ethyl 4-methylbenzenesulfonate (498 mg, 1.57 mmol)

and K_2CO_3 (0.5 g, 3.76 mmol) into dried 100-mL round flask all together. The reaction lasted overnight under Ar atmosphere at 90 °C. Quenching with H_2O and extraction is performed with ethyl acetate. Product (340 mg, 95 %) was obtained through purification using ethyl acetate and methanol (9:1 v/v). ^1H NMR ($CDCl_3$) δ [ppm]: 10.19(s.2H, -CHO), 7.54(s.2H, Ar-H), 4.31(t.4H, -OCH_2), 3.77(t.4H, -OCH_2), 3.52-3.55(m.16H, -OCH_2), 3.40(s.6H, -CH_3).

2-(4-(Diethylamino)phenyl)acetonitrile (4). Synthesis procedure was same as that mentioned above in 2.2.1 Synthesis part.

(2Z,2'Z)-3,3'-(2,5-bis(2-(2-(2-methoxyethoxy)ethoxy)ethoxy)-1,4 phenylene)bis(2-(4-(diethylamino)phenyl)acrylonitrile) (β-EODEADCS). The mixture of 2-(4-(diethylamino)phenyl)acetonitrile (102 mg, 0.55 mmol) and 2,5-bis(2-(2-(2-methoxyethoxy)ethoxy)ethoxy)terephthalaldehyde (100 mg, 0.22 mmol) in tert-butyl alcohol (15 ml) was stirred at 50 °C. Potassium tert-butoxide (61 mg, 0.55 mmol) powder was dropped into the mixture and stirred for 2 hours. The resulting material was purified by column chromatography using ethyl acetate and n-hexane (1.5:1 v/v). Viscous red β-EODEADCS (110 mg, 63 %) was obtained. ^1H NMR ($CDCl_3$) δ [ppm]: 7.84(d.4H, Ar-H), 7.56(d.4H, Ar-H), 6.70(d.4H, Ar-H, -CH_2), 3.49-4.27(m.24 H, -OCH_2), 3.37(q.8H, -CH_2), 3.34(s.6H, -CH_3), 1.20(t.12H, -CH_3).

2,5-bis((17-(13-(2,5,8,11-tetraoxadodecyl)-2,5,8,11,15-pentaoxahexadecan-16-yl)-13-(2,5,8,11-tetraoxadodecyl)-2,5,8,11,15-pentaoxaoctadecan-18-

yl)oxy)terephthalaldehyde (5). Put 2,5-dihydroxyterephthalaldehyde (50 mg, 0.3 mmol), 13,21-di(2,5,8,11-tetraoxadodecyl)-2,5,8,11,15,19,23,26,29,32-decaoxatritriacontan-17-yl 4-methylbenzenesulfonate (606 mg, 0.6 mmol) and K_2CO_3 (0.5 g, 83 mmol) into dried 100-mL round flask all together. The reaction lasted overnight under Ar atmosphere at 90 °C. Quenching with H_2O and extraction is performed with ethyl acetate. Product (303 mg, 53 %) was obtained through purification using ethyl acetate and methanol (9:1 v/v). ^{1}H NMR ($CDCl_3$) δ [ppm]: 10.16(s.2H, -CHO), 7.51(s.2H, Ar-H), 3.86(d.4H, -OCH_2), 3.52-3.55(m.124H, -OCH_2), 3.40(s.24H, -CH_3), 3.29(d.24H, -OCH_2), 2.40(t.2H, bridge-H), 2.10(t.4H, bridge-H).

(2Z,2'Z)-3,3'-(2,5-bis((17-(13-(2,5,8,11-tetraoxadodecyl)-2,5,8,11,15-pentaoxahexadecan-16-yl)-13-(2,5,8,11-tetraoxadodecyl)-2,5,8,11,15-pentaoxaoctadecan-18-yl)oxy)-1,4-phenylene)bis(2-(4-(diethylamino) phenyl)acrylonitrile) (β-wedge DEADCS).

The mixture of 2-(4-(diethylamino)phenyl)acetonitrile (20 mg, 0.1 mmol) and 2,5-bis((17-(13-(2,5,8,11-tetraoxadodecyl)-2,5,8,11,15-pentaoxahexadecan-16-yl)-13-(2,5,8,11-tetraoxadodecyl)-2,5,8,11,15-pentaoxaoctadecan-18-yl)oxy)terephthalaldehyde (100 mg, 0.05 mmol) in tert-butyl alcohol (15 ml) was stirred at 50 °C. Potassium tert-butoxide (15 mg, 0.1 mmol) powder was dropped into the mixture and stirred for 2 hours. The resulting material was purified by column chromatography using ethyl acetate and n-hexane (1.5:1 v/v). Viscous liquid β-EODEADCS (50 mg, 42 %) was obtained. ^{1}H NMR ($CDCl_3$) δ [ppm]: 7.80(d.4H, Ar-H), 7.52(d. 2H, Ar-H), 7.35(d.4H, Ar-H),

6.70(d.2H, -CH_2), 3.37-3.61(m.164H, -OCH_2, -CH_2), 3.36(s.6H, -CH_3), 1.20(t.12H, -CH_3).

3.2.2 Spectroscopic Characterization

^{1}H-NMR spectrum was recorded on a Bruker, Avance-300 (300 MHz) in $CDCl_3$ solution. Mass spectra were measured on a JEOL, JMS 600W spectrometer using electron impact (EI) or chemical ionization (CI), and JEOL JMS AX505WA spectrometer using fast atom bombardment (FAB) method. Significant fragments are reported in the following fashion: *m*/*z* (relative intensity). Elemental analysis was carried out using a CE instruments, EA1110 elemental analyzer. UV-visible absorption spectra were recorded on a Shimazu, UV-1650 PC spectrometer. Photoluminescence emission and excitation spectra were obtained using a Photo Technology International, Felix32 QM-4 and a Varian, Cary Eclipse Fluorescence spectrophotometer, correcting the spectra for the sensitivity of the detection system and the characteristics of the lamp, respectively. The absolute photoluminescence quantum efficiencies of the powder, crystal samples were measured using integrating sphere (Labsphere Co., 600 diameter). Relative fluorescence quantum yield was measured using Rhodamine 6G in ethanol as the standard. Time-resolved fluorescence lifetime experiments were performed by the time-correlated single photon counting (TCSPC) technique with a FluoTime200 spectrometer (PicoQuant) equipped with a PicoHarp300 TCSPC board (PicoQuant) and a PMA182 photomultiplier (PicoQuant). The excitation source was a 377 nm picoseconds pulsed diode laser (PicoQuant, LDH375) driven by a PDL800-D driver (PicoQuant) with fwhm ~70 ps. The multi-exponential least square fitting procedure was carried out with the Fluofit

software (PicoQuant), taking into possible double excitations of the IRF within the deconvolution. Fluorescence imaging with Live Cancer Cells: HeLa cells were cultured in Dulbecco's modified Eagle medium with 10% FBS, 5 mM L-glutamine, and 5 μg / mL gentamicin in a humidified 5% CO2 incubator at 37°C. Cells were seeded onto 35 mm cover glassbottom dishes and allowed to grow until a confluence of 70%. Prior to experiments, cells were washed twice with PBS (pH 7.4) to remove the remnant growth medium and then incubated in a serum-free medium (1.8 mL) containing samples (200 μL). For flluorescence imaging, the labeled cells were then washed twice with PBS (pH 7.4) and directly imaged using a LEICA DMI3000B equipped with a Nuance FX multispectral imaging system (CRI, USA).

3.2.3 Thermal analysis and Morphological analysis

Differential scanning calorimetry (DSC) was performed on a Perkin Elmer DSC7 at a heating rate of $10^{o}C\ min^{-1}$. FE-SEM images of nanoparticles were acquired on a JSM-6330F (JEOL). The samples were obtained by dropping the suspension of nanoparticles solution onto the glass substrates and drying it overnight in ambient conditions. Nanoparticles were prepared by simple precipitation method without surfactants. In this method, water was used as a non-solvent for materials in THF solutions. 99 % volume fraction of water was added into materials (2×10^{-5} M) in solution and then evaporation was conducted.. Nano-sized particles were formed spontaneously.

3.2.4 Quantum chemical calculation

Single molecule calculations were performed at the density functional theory (DFT) level of theory with the Gaussian09 software. Herein, the ground state geometry in the gas phase was fully optimized using B3LYP functional and 6-31G** basis set.

3.3 Results and Discussion

3.3.1 Photophysical property and Solvatochromism

Prior to study of photoluminescent property in solid state, we first determined the properties of newly synthesized β-EODEADCS and β-wedge DEADCS in solution and nanoparticles, comparing to optical properties of β-MODEADCS. The absorption and emission spectra in both THF solution and nanoparticles of β-MODEADCS, β-EODEADCS and β-wedge DEADCS are presented in Figure 3.3. In emission spectra, three compounds show intrinsic strong fluorescence property and similar fluorescence λ_{max} at 503 nm and in the isolated molecular state in solution. Upon nanostructure formation, the fluorescence maximum wavelength (λ_{max}) is red-shifted by 135 nm for β-MODEADCS, 66 nm and 50nm are shifted for β-EODEADCS and β-wedge DEADCS respectively in comparison with that of solution. The bathochromic fluorescence shifts are attributed to an increase in effective π-conjugated length through the aggregation-induced planarization.[3] Interestingly, however, absorption peak shift is different in self-assembled state depending on aggregation morphology. While β-MODEADCS displays blue-shifted absorption maximum change (λ_{max} = 20 nm) indicating a typical H-aggregation of linear chromophores, β-EODEADCS and β-wedge DEADCS exhibit red-shifted (about 10 nm and 25 nm) absorption maximum from that of solution upon J-aggregation formation. For exploring additional solid-state

properties, we also studied optical property and structural analysis of β-EODEADCS in powder state. But, we have no choice to analyze solid state properties of β-EODEADCS because β-wedge DEADCS is viscous liquid. Figure 3.4 depicts the emission and absolute fluorescence quantum yield of β-MODEADCS in powder. The intense fluorescence maximum wavelength is observed at 687 nm in far-red region with excellent quantum yield (Φ_{FL} = 0.6). This emission wavelength longer than that of nanoparticles is related to the formation of specific stacking structure associated with the electronic and geometrical characteristics of the molecule in each condition. Thus, we analyzed the molecular stacking structure by powder XRD. X-ray diffraction (XRD) pattern of β-EODEADCS powder implies that several crystalline direction is existed based on other peaks except for (100), (200), (300) peak. The slipped crystal lattice is observed according to the relative intensity change of preferred orientation in XRD patterns, which is resulted from substitution of more bulky ethylene oxide group.

Because the molecular structure consists of donor part and acceptor part alternately, solvatochromism of absorption and emission has been studied by Lippert-Mataga model,[4] in a series of solvents with various polarity. As shown in Figure. 3.7, the solvatochromism in absorption is very weak or negligible for β-EODEADCS since net dipole moments of the ground and locally excited (LE) states should be almost cancelled due to the high level of geometrical symmetry. On the other hand, fluorescence maximum frequencies show strong positive solvent-polarity dependence, suggesting that intramolecular charge transfer (ICT) from the LE state produces a polar

excited state affected by the molecular environment.[5] Therefore, D-A-D-A-D type β-EODEADCS exhibits strong solvatochromic color tuning of fluorescence largely shifted from the green to red spectral region.

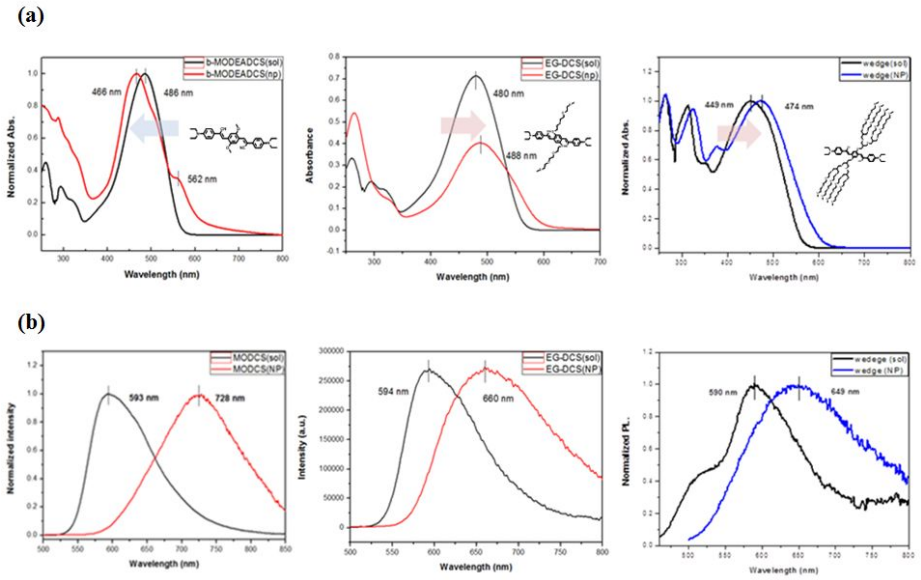

Figure 3.2. (a) UV-Visible absorption and (b) Photoluminescence spectra of β-MODEADCS, β-EODEADCS and β-wedge DEADCS in THF solution (c = 2 x 10^{-5} mol L^{-1}) and THF/water mixture or water (c = 2 x 10^{-5} mol L^{-1}).

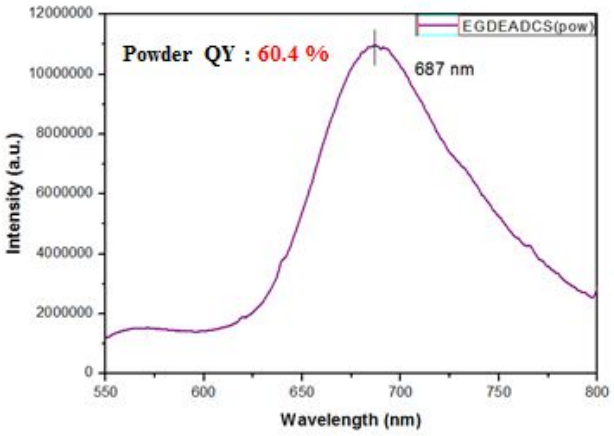

Figure 3.3. Photoluminescence spectrum and absolute fluorescence quantumn yield of β-EODEADCS in powder.

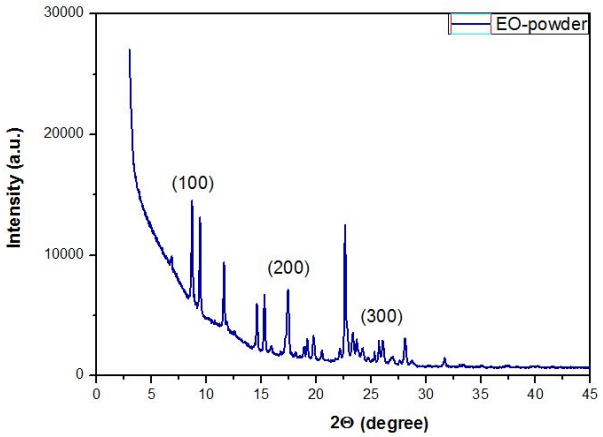

Figure 3.4. Powder XRD data of β-EODEADCS.

Figure 3.5. Image of β-EODEADCS solvatochromic behavior.

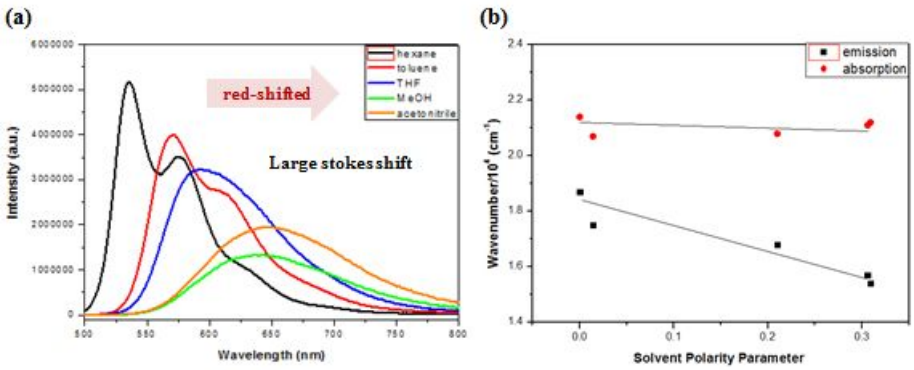

Figure 3.6. (a) Photoluminescence spectra of β-EODEADCS in various solvent with different polarity ((c = 2 x 10^{-5} mol L^{-1}) and (b) A plot of the absorption and emission maxima of β-EODEADCS solutions as a function of solvent polarity parameter of the Lippert-Mataga model. Solvent parameter $(\Delta f) = \{(\varepsilon - 1) / (2\,\varepsilon + 1) - (n^2 - 1)/(2n^2 + 1)\}$, where ε is the dielectric constant and n is the refractive index.

3.3.2 Fabrication of self-assembled nanostructures and Morphology

The nanoparticles of β-EODEADCS for aqueous systems were fabricated with the following two precipitation methods. First, the stock solution of β-EODEADCS in BHT-free tetrahydrofuran was prepared with concentration of 10^{-3} mol L^{-1}. The 100 μl solution was dropped into the vigorously stirred 10 mL water in 20 ml volume glass vial and well-mixed with vortex mixer. The uniform nanoparticles were obtained after removing tetrahydrofuran by evaporation under reduced pressure. Second, the stock solution using BHT-free tetrahydrofuran was prepared as mentioned above. The tetrahydrofuran was then removed and dried solid-state material was obtained. After that, water is poured into the vial and it was shakened by vortex mixer for 90 seconds. Upon addition of the water, the β-EODEADCS molecule aggregated and formed nanoparticles instantly. Through the observation of uniform nanoparticles formation using simple two reprecipitation methods, β-EODEADCS including hydrophilic ethylene oxide group has appropriate compatibility with water. The morphology of β-EODEADCS nanoparticles was studied by field-emission scanning electron microscopy (FE-SEM) and clearly distinguished spherical shape of nanoparticles could be observed in Figure 3.8 (a). Dynamic light scattering (DLS) results suggest a narrow particle size distribution and the volume average hydrodynamic diameter of β-EODEADCS nanoparticles is 117 ± 25 nm (See Figure 3.8 (a)). Additionally, as shown in Figure 3.9, there is small overlap between absorption and emission spectra of β-EODEADCS nanoparticles, which is

beneficial to the confocal fluorescence image in overcoming interferences of optical absorption and autofluorescence of biological media.

In case of β-wedge DEADCS, it forms self-assembled nanostructures without organic solvent and surfactants. Cryogenic transmission electron microscopy (cryo-TEM) reveal that β-wedge DEADCS based on wedge type of bis(ethylene oxide) chain self-organizes into planar sheets in 0.03 wt % aqueous environment (See Figure 3.8 (b)). Its large planar sheets can be attributed to strong tendency of the rod segments to effectively pack with an anisotropic arrangement through π−π stacking interactions.

Previously, in case of β-MODEADCS nanoparticle formation, we observed that larger size of particles (about 220 nm) was fabricated without polymer matrix due to rigid and hydrophobic molecular backbone. However, relative smaller size of nanoparticles (112 nm) was formed by means of F68. Although the advantages of self-assembled capability, β-EODEADCS still show shorter wavelength fluorescence (λ_{max} = 660 nm) compared to β-MODEADCS nanoparticles emission. (λ_{max} = 725 nm). For realization of Near Infra-Red fluorescence in biological sysyem, we devised a new strategy, which is fabricating co-nanoparticles composed of β-EODEADCS and β-MODEADCS. Because intermolecular interaction between two different molecules is very important to make self-assembled co-nanoparticles, we employed β-EODEADCS and β-MODEADCS having same molecular backbone for better interaction between them. It was also expected that amphiphilc β-EODEADCS could surround the extremely hydrophobic β-MODEADCS, thereby facilitating the nanoparticles formation without assistance of other

biocompatible surfactants. The co-nanoparticles for aqueous environment were fabricated with the following method. The stock solution with concentration of 10^{-3} mol L^{-1} was prepared varying each materials ratio and sonicated for well-mixed composition. The 100 μl solution was then dropped into the vigorously stirred 10 mL water. Co-assembled nanoparticles were formed spontaneously after evaporation tetrahydrofuran and sonication.

These are intriguing results that have advantages for practical biological application. Consequently, we decided to conduct In Vitro cellular imaging by using far red fluorescent self-assembled β-EODEADCS nanoparticles and co-nanoparticles with proper particle size. Through the experiment, we proved the validity of our molecular design strategy for biological environment.

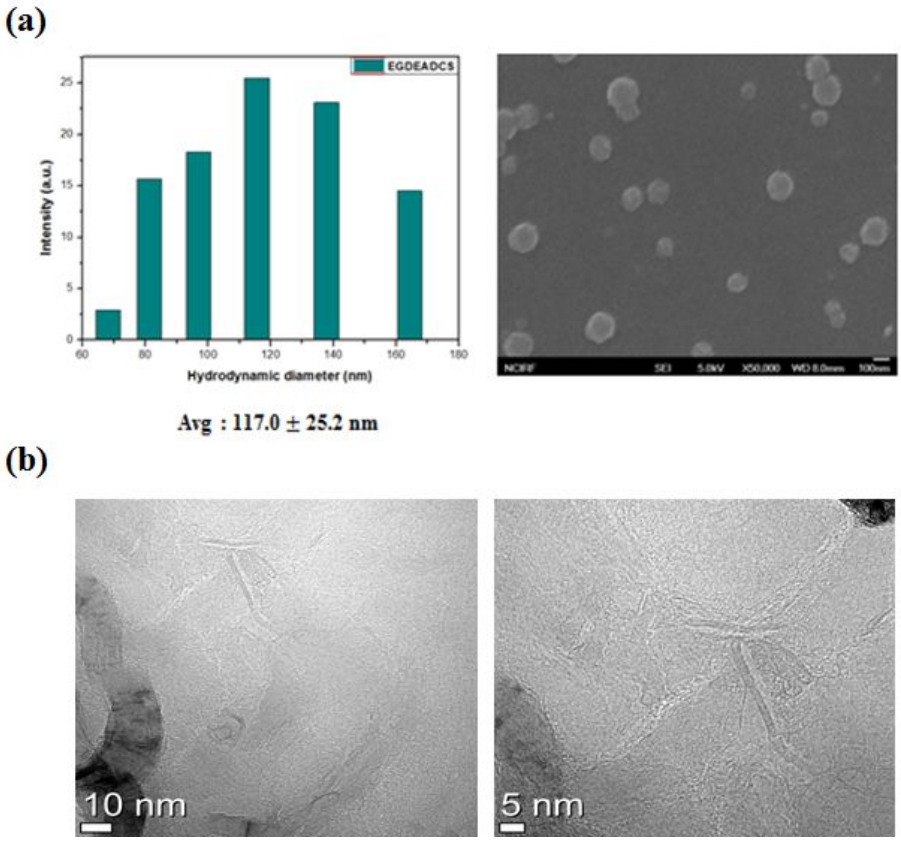

Figure 3.7. (a) Dynamic light scattering (DLS) data and FE-SEM image of β-EODEADCS in water (b) Cryo-TEM image of β-wedge DEADCS obtained from a 0.03wt% aqueous solution.

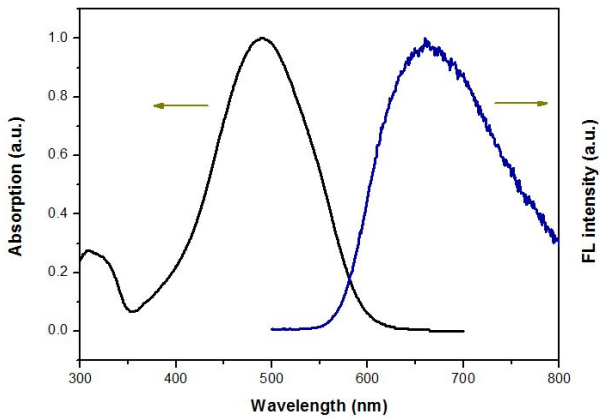

Figure 3.8. UV-vis absorption and photoluminescence spectra of β-EODEADCS nanoparticles in water at room temperature (excited at 480 nm).

3.3.3 In vitro Cell imaging

To explore of novel far-red and Near Infra-Red fluorescent probes with high biocompatibility, efficient emission property, and strong photobleaching resistance is highly desirable for bioimaging.[6] Recently, organic fluorophore-loaded nanoparticles have recently emerged as a new generation of fluorescent nanoprobes because of the synthetic versatility and facile surface functionalization for specific targeting. Until now, only a few materials possessing not only self-assembly behaviors but also far-red to Near Infra-Red fluorescence have been reported. Therefore, to design and synthesize new materials with two phenomena is meaningful and remains as an important challenge.

The application of the self-assembled β-EODEADCS nanoparticles in vitro cellular imaging was studied using a LEICA DMI3000B equipped with a Nuance FX multispectral imaging system. After incubation with the β-EODEADCS nanoparticle suspension ($c = 1 \times 10^{-4}$ mol L^{-1}) for 2 hours at 37 ^{o}C in the culture medium, the cells were imaged with a 460 $\pm$ 20 nm laser excition and fluorescence signals from the cells were collected from 500 nm to 750 nm. It was observed that nanoparticles of β-EODEADCS itself are possible to cell internalization successfully, showing intense self-signaling fluorescence from cytoplasmic regions with its own spectral signature in Figure 3.10. Whereas β-EODEADCS nanoparticles exhibit deep-red fluorescence (λ_{max} = 660 nm) before internalization into the cell, loaded β-EODEADCS nanoparticles show unexpected orange fluorescence. This

phenomenon is attributed to the liphophilic environment in the cell making molecules loose in the nanoparticles. Thus, for proper far-red and Near Infra-Red fluorescent bioprobes for cell-imaging, co-nanoparticles consisting of β-EODEADCS and β-MODEADCS with different ratio and same overall concentration were also demonstrated. The uptake time of samples to the cells was 1 hour at 37 ^{o}C and cells were imaged by the excitation of co-assembled nanoparticles at 460 $\pm$ 20 nm. Interestingly, it was found that maximum of emission wavelength was red-shifted about 60 nm (λ_{max} = 600 nm) and co-nanoparticles were clearly internalized in HeLa cell cytoplasm (Figure 3.11). This result implies that β-MODEADCS plays a role as a molecular glue by compact and rigid molecular structure, which tighten the nanoparticle efficiently. In addition, amphiphilic β-EODEADCS shows the capability as a nanocarrier base on the failure of bare β-MODEADCS nanoparticles internalization for cell imaging. It is reasonable to design new materials based on attachment of ethylene oxide moiety with appropriate length, in terms of several points such as low cytotoxicity, good water solubility, and maintained bright fluorescence.

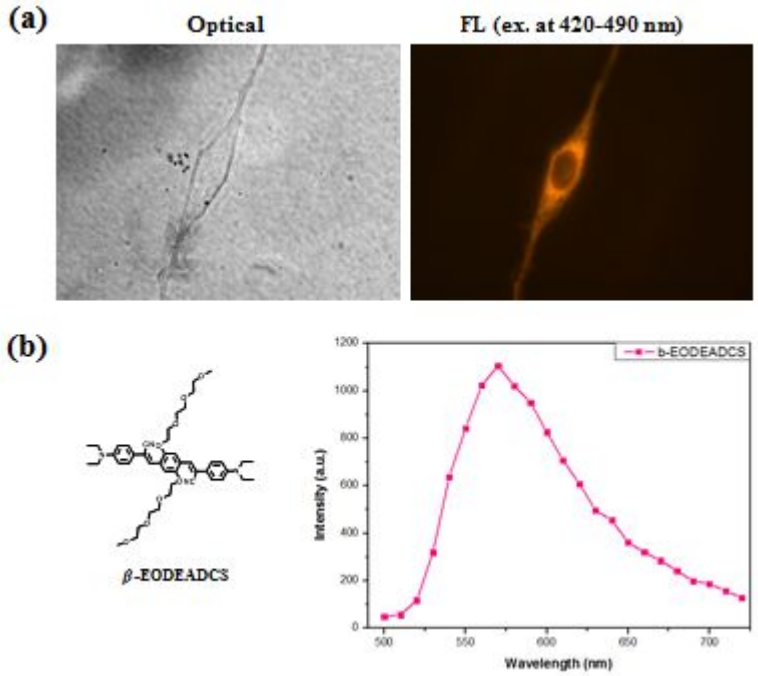

Figure 3.9. (a) Optical and fluorescence (FL) images of HeLa cells tereated with β-EODEADCS nanoparticles (b) Localized fluorescence spectra from the cytoplasmic regions.

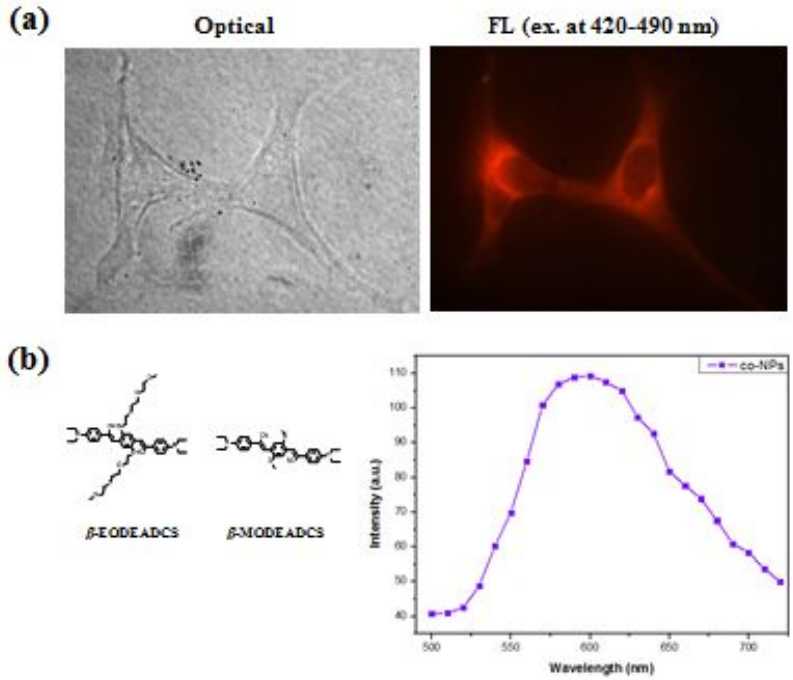

Figure 3.10. (a) Optical and fluorescence (FL) images of HeLa cells tereated with co-nanoparticles of β-EODEADCS : β-MODEADCS (8:2) volume ratio (b) Localized fluorescence spectra from the cytoplasmic regions.

3.4 Conclusion

In summary, we have synthesized laterally grafted amphiphilic β-dicyanodistyrylbenzene based β-EODEADCS and β-wedge DEADCS successfully and characterized intense far-red fluorescence emission of β-EODEADCS in the solid state. Also, we investigated their aggregation behavior of laterally grafted amphiphilic rod molecules. β-EODEADCS forms unique stacking structure in aggregated state through the various secondary bonding interaction by introducing linear hydrophilic ethylene oxide moieties into the core vertically and shows high fluorescence in far-red and Near Infra-Red region (Φ_{FL} = 0.6). To further study of aggregate behavior, their morphologies in aqueous solution were obtained by diverse experiments. Whereas β-EODEADCS showed self-assembled spherical nanoparticles without aid of polymer surfactants and narrow size distribution, β-wedge DEADCS formed sheet-like structure spontaneously in which hydrophilic oligoether dendrons are attached to hydrophobic β-DCS molecular backbone. Additionally, we clearly demonstrated the great potential of β-EODEADCS as a far-red fluorescent probe through in vitro cellular imaging studies using HeLa cells. While β-EODEADCS nanoparticles exhibit orange fluorescence with an emission peak (λ_{max} = 600 nm), largely red-shifted emission (λ_{max} = 660 nm) is obsereved in case of co-nanoparticles using β-EODEADCS and β-MODEADCS in the cell. With red-Near Infra-Red emission property, biocompatible self-assembled

nanoparticles may find more applications in both fundamental and practical research on living systems. The organic nanoparticles based on amphiphilic β-dicyanodistyrylbenzene derivatives provide a new strategy to construct red fluorescent probes.

3.5 Bibliography

1. a) M. Lee, B. K. Cho, W. C. Zin, Chem. Rev., **2001**, 101, 3869; b) J. H. Ryu, N. K. Oh, W. C. Zin, M. Lee, J. Am. Chem. Soc., **2004**, 126, 3551; c) J. H. Ryu, D. J. Hong, M. Lee, Chem. Commun., **2008**, 1043.
2. S. Shin, S. H. Gihm, C. R. Park, S. Kim, S. Y. Park, Chem. Mater., **2013**, 25, 3288.
3. a) H. Bassler, B. Schweitzer, M. A. El-Bayoumi, Pure Appl. Chem., **1965**, 11, 371; b) K. Pichler, D. A. Halliday, D. D. C. Bradley, P. L. Burn, R. H. Friend, A. B. Holmes, J. Phys.: Condens. Matter., **1993**, 5, 7155; c) F. Wurthner, T. E. Kaiser, C. R. Saha-Moller, Angew. Chem. Int. Ed., **2011**, 50, 3376.
4. W. Baumann, H. Bischof, J.-C. Frohling, C. Brittinger, W. Rettig, K. Rotkiewicz, J. Photochem. Photobiol. A, **1992**, 64, 49.
5. a) M. A. Albota, C. Xu, W. W. Webb, Appl. Opt., **1998**, 37, 7352; b) F. C. Krebs, H. Spanggard, J. Org. Chem., **2002**, 67, 7185.
6. a) R. Weissleder, Nat. Biotechnol., **2001**, 19, 316; b) J. V. Frangioni, Curr. Opin. Chem. Biol., **2003**, 7, 626; c) C. Tung, Y. Lin, W. Moon, R. Weissleder, ChemBioChem., **2002**, 3, 784.

초 록

고효율의 근적외선 영역의 발광특성을 보이는 베타 다이사이아노다이스티릴벤젠 유도체들의 합성, 특성분석, 그리고 응용에 관한 연구

김 민 아

재료공학부

The Graduate Scool

Seoul National University

최근 근적외선 영역에서 형광을 보이는 π-공액 유기물질은 대부분 전자 주게와 전자 받게를 포함한 분자구조나 확장된 컨쥬게이션에 의한 평평한 구조를 가짐으로써 강한 분자간의 π-π 상호작용에 의해 형광이 소광 되는 특징을 보인다. 그러나 강한 고체상의 근적외선 영역에서의 형광을 보이는 물질들은 바이오센서, 레이저, 유기발광 다이오드 등의 넓은 분야에 적용이

가능하기 때문에 이러한 특성을 보이는 물질에 대한 연구는 의미 있고 도전적인 분야이다.

본 연구에서는, 근적외선 영역에서 고발광성 베타-다이사이아노다이스티릴벤젠 유도체들을 체계적으로 설계하고 성공적으로 합성하였다. 그리고 광학적, 구조적, 광물리적 분석법을 이용하여 합성한 물질들의 고체상에서 근적외선 영역의 강한 형광 특성 및 분자의 적층 조립구조를 조사하였다. 이 중, β-MODEADCS는 C-H···O, C-H···π, 그리고 C-H···H-C 상호작용에 의해 단결정을 형성하고 가장 장파장인 710 nm 에서의 최대 발광을 했다. 그리고 기계적 자극에 의한 구조 및 형광 변화, 열에 의한 회복에 대해 XRD와 열적, 광학적 분석법으로 확인 하였다. 또한, 분자 중심 부분을 친수성 유닛으로 치환한 물질들 중 β-EODEADCS는 역시 강한 적색 형광을 고체상에서 발하였고, 물의 환경에서 간단한 재침전법으로 자기조립에 의해 둥근 나노입자를 형성하는 반면 액상인 β-wedge DEADCS는 β-EODEADCS와 달리 nanosheet의 독특한 구조체를 형성하는 것을 확인할 수 있었다. 마지막으로, β-EODEADCS의 이러한 자기조립적 나노구조체 형성 능력과 적색 형광을 활용하여 성공적으로 생체 외 이미징 (in vitro imaging)을 할 수 있었다.

주요어 : 베타−다이사이아노다이스티릴벤젠, 강한 형광, 적색 형광체, 기계적 힘에 의한 변색성, 고체상, 생물학적 이미징

학 번 : 2012-22535

List of Presentation

김민아, 서장원, 박수영, "Synthesis and Properties of Near Infra-Red Fluorescent MODCS Derivatives", 15th Asian Chemical Congress, August 19-23, 2013, Singapore.

김민아, 서장원, 박수영, "Synthesis and Properties of Near Infra-Red Fluorescent N-amine Functionalized β-Dicyanodistyrylbenzene (DCS) Derivatives", 9th Korea-Japan Symposium on Frontier Photoscience, November 24-27, 2013, Seoul National University.